BEA
Bureau d'Enquêtes et d'Analyses
pour la sécurité de l'aviation civile
www.bea.aero
@BEA_Aero

TECHNICAL REPORT

Accident to the Airbus A380 registered F-HPJE and operated by Air France on 30/09/2017 en route over Greenland

June 2018 - June 2019
Phase III field campaign and part extraction

RÉPUBLIQUE FRANÇAISE
Liberté
Égalité
Fraternité

Published : June 2020

EXECUTIVE SUMMARY

Following the engine No. 4 failure which occurred to the Airbus A380-861, registered F-HPJE, en route over Greenland on 30 September 2017, the Danish Accident Investigation Board (AIB DK) opened a safety investigation and delegated it to the BEA. The BEA represents France, State of Operator, State of Registry and State of Design of the aircraft. Investigators from AIB DK, representing Greenland (autonomous constituent country of the Kingdom of Denmark), State of Occurrence, from NTSB, representing the United States of America, State of Engine Manufacturer, and BST-TSB, representing Canada, State where the flight crew diverted and landed safely, took part in this safety investigation.

Technical advisors from the aircraft manufacturer Airbus, from the operator Air France and from the engine manufacturer Engine Alliance (which is a Joint Venture between General Electric and Pratt & Whitney) were also involved in this investigation.

The Airbus A380-861, operated by Air France, was performing a flight from Paris (France) to Los Angeles (United States of America) under the call-sign AF066. It had taken off from Paris Charles de Gaulle Airport on Saturday, 30 September 2017 at around 09:30 (UTC), with 497 passengers and 24 crew members on board. Following a failure on the No. 4 engine while the plane was climbing to FL370, the flight crew diverted to Goose Bay Airport (Canada), where they landed at 15:42 (UTC) without any further incident.

Damage to the aircraft was confined to the No. 4 engine and its immediate surroundings. A visual check of the engine had found that the fan, the first rotating assembly at the front of the engine, had failed and along with the air inlet and fan case, had separated in flight. The data contained in the flight data recorder (FDR) was used to determine the aircraft's track and position when the failure of the No. 4 engine occurred and to demarcate a search area to find the parts which had separated from the aircraft.

A previous report, published in May 2019 (BEA, 2019)[(1)], described the first two search phases:

- Phase I which consisted in the search and recovery of visible parts laying on the ice sheet. It started immediately after the event and ended on 12 October 2017, i.e. 12 days after the accident,
- Phase II, made up of two consecutive operations:
  - an aerial campaign (Greensar), consisting in the use of synthetic aperture radars (SAR) operated by ONERA from an airplane belonging to AVDEF, to try to detect and locate the missing parts on the ice sheet under snow and ice layers,
  - a ground campaign (Camp Recovery) led by GEUS, consisting in the survey of the targets provided by ONERA from the aerial campaign and then in performing a systematic search with the help of ground penetrating radars (GPR) as the target survey was inconclusive.

[(1)] https://www.bea.aero/uploads/tx_elyextendttnews/F-HPJE_TECHNICAL_REPORT.pdf

Despite the amount of work and effort invested in the operations described above, the fan hub fragments were not reliably detected at the end of June 2018. The data gathered during Phase II were closely analyzed and led to additional efforts being considered.

ONERA continued to process the radar data acquired during the Greensar operation after having headed back to France. New specific algorithms made it possible to detect the test hub (a test part intentionally buried close to the search area for detection test purposes) with the X-band radar frequency, which gave a more promising result than what was deemed possible just after the flight campaign. At the end of their work, one high-confidence and two lower-confidence targets were identified in or very close to the search area. Also, parts that were spotted on site during Phase I but not recovered were rendered visible with the X-band radar data in the light debris area (upstream from the location of the event).

At the same time, the ground search and recovery team considered that it was necessary to test new ground sensors with a larger swath and a more reliable response, if new ground searches were to happen in 2019.

Meanwhile, Engine Alliance performed dynamic Finite Element simulations of a fan hub fracture, and obtained refined predicted data regarding the characteristics of the fan hub fragment (mass and ejection velocities in particular) based on a bore to rim fracture of the hub. New ballistic computations were carried out with this refined data, in order to try to determine a high probability search area, smaller in size than the first search area, in case systematic ground searches with no new potential targets had to be re-launched.

All these tasks were completed at the end of 2018. Following the availability of new promising ONERA targets and the development of a new electromagnetic sensor, a decision about going back to the ice sheet was made at the end of February 2019, for a spring field campaign planned in May 2019.

The spring field campaign (phase III) was complicated by weather hold-ups, but a ground detection was finally obtained at the high-confidence target location at the very end of the campaign. An extraction campaign was organized, which took place in June 2019. The sum of these efforts resulted in one of the fan hub fragments, with blades attached, being recovered and extracted for further metallurgical examination, on 30 June 2019.

The purpose of this report is to present the different tasks carried out during the year June 2018 – June 2019 including the phase III field campaign and the extraction phase.

These tasks were the following (see Fig. 1):

- Definition of search area for Phase III
  - engine failure simulation
  - ballistic computation updates
  - radar imagery data[(2)] analysis

[(2)] Data from Phase II.

- Evaluation of new detection capabilities
  - RECCO®[3]
  - sniffer dogs
  - Electro-Magnetic (EM) sensors
- Phase III field campaign and part extraction

A final chapter is proposed to discuss the lessons learned during the 21-month search period with a view to sharing experience and facilitating further searches in case a similar event should occur again.

[3] RECCO® rescue system is an electronic method of finding people buried in an avalanche or lost in the outdoors.

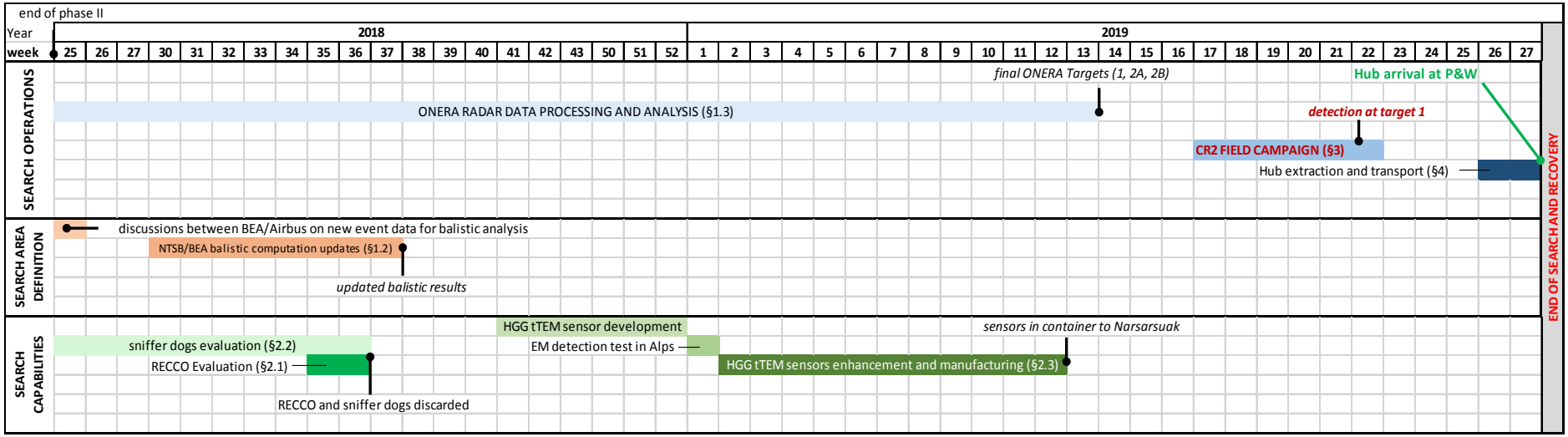

Fig. 1: Timetable of search phase III, from June 2018 to end of operations[4]

[4] HGG : HydroGeophysics Group from the Department of Geosciences of Aarhus University.
tTEM: ground-based towed transient electromagnetic data acquisition system developed by HGG.

TABLE OF CONTENTS

EXECUTIVE SUMMARY 2

TABLE OF ILLUSTRATIONS 8

1 - DEFINITION OF SEARCH AREA FOR PHASE III 11

1.1 Engine failure simulation 11

1.2 Ballistic computation updates 13

1.2.1 Refined data 13

1.2.2 Ballistic computation updates 19

1.3 Radar imagery data analysis 24

1.3.1 General 24

1.3.2 Motivation of massive multilooking 24

1.3.3 Technical difficulties for massive multilooking 26

1.3.4 (Absolute) image registration issues 26

1.3.5 Registration depth issues 27

1.3.6 Surface motion issue 27

1.3.7 SNR (noise & clutter) evaluation issues 28

1.3.8 Results 29

1.4 Optical satellite imagery 31

2 - EVALUATION OF NEW DETECTION CAPABILITIES 34

2.1 RECCO 35

2.2 Sniffer dogs 36

2.3 Electro-Magnetic (EM) sensors 37

2.3.1 tTEM description and ways of improvement 38

2.3.2 SnowTEM development and testing 40

2.3.3 Conclusion on the EM sensor evaluation 45

2.4 Conclusion regarding detection means and field campaign strategy 46

3 - PHASE III FIELD CAMPAIGN – CAMP RECOVERY 2 47

3.1 Logistics and planning 47

3.2 Ground search campaign 49

3.3 Positive signal response 52

4 - EXTRACTION 54

4.1 Overview 54

4.2 Development of campaign 54

5 - LESSONS LEARNED **59**

5.1 Safety 59

5.2 Organization 61

5.3 Means of detection 62

5.4 Extraction 67

5.5 Weather conditions 68

6 - CONCLUSION **69**

REFERENCES **71**

TABLE OF ILLUSTRATIONS

Fig. 1: Timetable of search phase III, from June 2018 to end of operations. 5

Fig. 2: Hub "bore to rim" fracture scenario simulated by removing hub elements in blade slot 11

Fig. 3: Simulation of fan hub "bore to rim" failure is consistent with damage observed on event engine (source: EA) 12

Fig. 4: Simulation results of the fan hub bore to rim rupture scenario, consistent with damage observed on engine (source: EA) 13

Fig. 5: Comparison between GPS (blue) and IRS (purple) position data at Goose Bay (top) and Paris Charles-De-Gaulle (bottom) 14

Fig. 6: Computation of FMS data from GPS and IRS data (source: Airbus) 15

Fig. 7: Comparison of event positions: updated (FMS) location of event (light blue), initial BEA (GPS) event position (dark blue), Airbus position taken into account for Ariane computations (white). Green line is FMS trajectory, purple line is IRS trajectory. 15

Fig. 8: Comparison between barometric altitude (blue) and GPS altitude (orange) 16

Fig. 9: Altitude data recorded at time of engine failure (13:49:18). 17

Fig. 10: NOAA data (source Airbus) showing temperature profile versus altitude at 12:00 UTC, 67.5°N, 315°W. Red line is standard ISA temperature lapse rate and blue line is reported temperature lapse rate at that date and time. 18

Fig. 11: Locus calculation for the two speeds (57 and 133 m/s) and the two angles of ejection (5 and 11 o'clock) from LS-Dyna simulation. 20

Fig. 12: Locus calculation for the two fragments. Each fragment was simulated leaving the engine with a radial angle vector corresponding to 4, 6 and 11 o'clock. 4 and 6 o'clock were chosen to mark off the probable position of the debris which exit at the 5 o'clock position, as there were uncertainties on the damage observed on the engine. Grey area is previous NTSB search area calculated in early 2018. 21

Fig. 13: Shifted search area (in red) based on late 2017 Ariane computations (in grey) 22

Fig. 14: Updated primary (red) and secondary (orange) search areas 23

Fig. 15: Final updated search area. Primary (red) area is 4.4 km^2, secondary (red + orange) is 8.10 km^2, and wide area after dilation (dark blue) is 17 km^2. 23

Fig. 16: Comparison of pixel level density function for clutter only in red and clutter + target at 10% clutter level in green for a single look (left) and 18 equivalent looks (right). For a given threshold, non–detections (ND) are represented by the green area and false alarms (FA) by the red area. 25

Fig. 17: 432 looks in X-band composite image assuming Lambertian clutter (left with contrast enhanced for emphasis of sub-swathes/look edge discontinuities), and assuming a clutter model deviating from Lambert's law as a degree 2 polynomial function of incident angle (right). 28

Fig. 18: Comparison of candidate #1 X-band profiles from opposed headings (233°, upper left hand side, 053°, upper right hand side. When comparing profiles of sub-images obtained from opposite imaging directions, the peak of intensity should match if the object is at the targeted depth (red dot, lower image). Features not at the targeted depth (here the low of intensity due to the crevasse air) do not match (grey arrows) because of perspective. 29

Fig. 19: Candidate (bright pixels) for fan hub fragment on the final X-band image with contrast enhancement for printing. The dark horizontal line is a crevasse under a 6 m snow bridge. 30

Fig. 20: Location of ONERA candidates 1, 2a and 2b with respect to search area 30

Fig. 21: Example of UHF-band image (vertical polarization) emphasizing the crevasses in the search zone (delimited by black line). Locations of ONERA candidates are marked by yellow plots. 31

Fig. 22: Pleiades images dated 28 May 2018 – flags are visible from space (two gray dots in lower right). A mismatch of 207 m is observed between real location of flags (blue squares, position recorded in the field via GPS) and satellite image position. 32

Fig. 23: Pleiades images dated 18 May 2018. No mismatch is observed between real location of flags as recorded in the field via GPS (blue dots) and flag location in satellite image (gray patches). 33

Fig. 24: Pleiades images dated 28 May 2018. Expected camp location marked with orange tent. Traces in the snow (blue oval) indicate the actual tent locations. 34

Fig. 25: Pleiades images dated 18 May 2018. Expected camp location marked with orange tent. Traces in the snow (blue oval) indicate the actual tent locations. 34

Fig. 26: most promising ONERA target location (blue dot) with background from Pleiades satellite image dated 11 October 2017. No part hub could be observed on the image in this area. 34

Fig. 27: Sniffer dog before (left) and after (right) dispatch on the ice sheet (source: AIB-DK) 37

Fig. 28: Picture of tTEM system and schematical overview of layout (source: HGG). 38

Fig. 29: Picture of test setup: test hub placed 2 m from center of transmitter frame (source: HGG). 38

Fig. 30: Signal measured during the tests in Funder. Source: HGG. 40

Fig. 31: Initial test location, "Breithorn Plateau" in center, with Breithorn (4,164 m), on left hand side. View from Klein Matterhorn. "Gobba di Rollin" ski lift is just visible on right hand side. Crevasses downstream of the plateau are clearly visible. 41

Fig. 32: Final location of the test site – closest ski lifts are shown with blue lines 42

Fig. 33: Location of power lines (red lines) and noise measurements (green dot). 43

Fig. 34: Signal measurement with SnowTEM - close to the powerline in Zermatt (green), far from the powerline in Zermatt (grey), and measurement in Funder (black). 44

Fig. 35: Snowmobile towing SnowTEM during the test in Zermatt in low visibility conditions in a snow storm. 44

Fig. 36: Digging out one of the two SnowTEM systems after a snowstorm. 48

Fig. 37: Base camp for ground search campaign – Photo: Rune Ellerup Kraghede. 50

Fig. 38: Location of target 1 signal (red circle), and nearby crevasses (four orange flags on left hand side and four black flags on right hand side). Photo is taken from west looking east. Crevasses run east/west. Crevasse locations outside of orange and black markers are uncertain. Distance from target center to edge of black-flagged crevasse is 2 m. Distance from target center to edge of orange-flagged crevasse is 5 m. Black-flagged crevasse width is 4 m, bridge thickness 6 m. Orange-flagged crevasse width is 4 m, thickness 8 m. Also barely visible in image running left/right near bottom are FrostyBoy tracks. Source: Thue Bording (HGG). 52

Fig. 39: Location of detection (red star) – yellow circles are ONERA target locations, white stripes are crevasses as seen on UHF images, red markings are crevasse edge detections. 53

Fig. 40: Weather forecast from 22 June on search site, windy.com 55

Fig. 41: Weather forecast from 27 June on search site, windy.com 55

Fig. 42: Photograph from helicopter of excavation work-site as described in (Mankoff, et al., 2020). (A and A') Dark red graphic overlays between flags mark known crevasse locations as detected by GPR and DGNSS. Dashed lines enclose safe areas and pink marks unsafe areas defined with GPR data, the UHF basemap (Fig. 21), extensive snow probing and crevasse location uncertainty with distance from known crevasse locations. (B) Ramp out of pit. (C) Plywood used to cover pit overnight to prevent drifting snow filling. (D) Safety rope bridging crevasse between the northern (far) camp island and the southern (near) work island. (E) Sled. (F) Winch and winch platform. (G) Generator used to power winch. (H) Bamboo poles marking polar bear alarm trip-wire surrounding sleep tent. (I) Herman Nelson heater, hose and fuel barrel. (J) Helicopter landing zone. Photo by Austin Lines. 56

Fig. 43: Melting out snow and ice around part in 4 m deep hole. Photo by Arnar Ingi Gunnarsson. 57

Fig. 44: Photo by Dirk van As, Greenland Guidance. Photo of Icelandic rescuer melting out fan hub. 58

Fig. 45: Loading of crate with fan hub into transport aircraft, an Antonov 12. 59

Fig. 46: Position of event and first areas of searches. Background is a Landsat 8 image of South Greenland. Yellow and red areas were provided to Air Greenland for helicopter survey. 59

Fig. 47: Pieces of debris found by Air Greenland (yellow plots). Foreground map is UHF image of search area acquired during air campaign of April 2018. Crevasses are clearly visible in white. The background is TerraSar X image of area. 61

Fig. 48: Frostyboy autonomous vehicle (source: Austin P. Lines – PRE) 64

Fig. 49: Towing MALÅ GPR with snowmobile during first field campaign (source: GEUS) 65

Fig. 50: Blowing snow burying equipment during a strong wind episode. 69

1 - DEFINITION OF SEARCH AREA FOR PHASE III

1.1 Engine failure simulation

At the end of June 2018, Engine Alliance presented detailed information provided by the LS-Dyna fan hub failure simulation. Engine Alliance created a LS-Dyna model of the GP7000 Fan Module to assess the different likely failure scenarios and to provide insight into hardware findings and progression of the failure of the event. The model consisted of a low pressure rotor system (fan case, intermediate case, low pressure compressor, including the static casing structure), low pressure turbine, and the low pressure rotor bearing supports.

The LS-Dyna model consists of several physical finite element models. These models are based on calibrated material models (elasticity, visco-plasticity and damage mechanics) as well as modelling techniques and procedures. They have been validated in Pratt & Whitney engine development programs through the correlation of model results with test results, for Fan Blade Off and Bird Ingestion conditions. The material models used in this analysis are elastic-plastic. Failure allowables for selected materials are turned on to allow the simulated fracture of engine components. As noted above, the model is not a full engine model, but consists of a sub-set of engine hardware with a goal of evaluating the fan hub behavior and its local surroundings in the fan module. Because of this limitation, results from the simulations are considered valid for only the initial 20 to 30 milliseconds, which capture the time from initial part fracture until roughly the time at which the hub fragments penetrated the fan containment case (for the cases where the hub ruptured).

The LS-Dyna simulation aimed to understand the dynamic of the dispersion of the engine pieces following a hub failure. Since LS-Dyna is not a fracture mechanics analysis, it was necessary to analytically start the event by forcing the initial fracture in the model. As such, the simulation starting point hypothesis was to consider a bore to rim fracture (Fig. 2). This was not considered as the unique likely failure scenario but it made it possible to simulate a complete rupture of the hub. This was done numerically by removing hub elements in a blade slot.

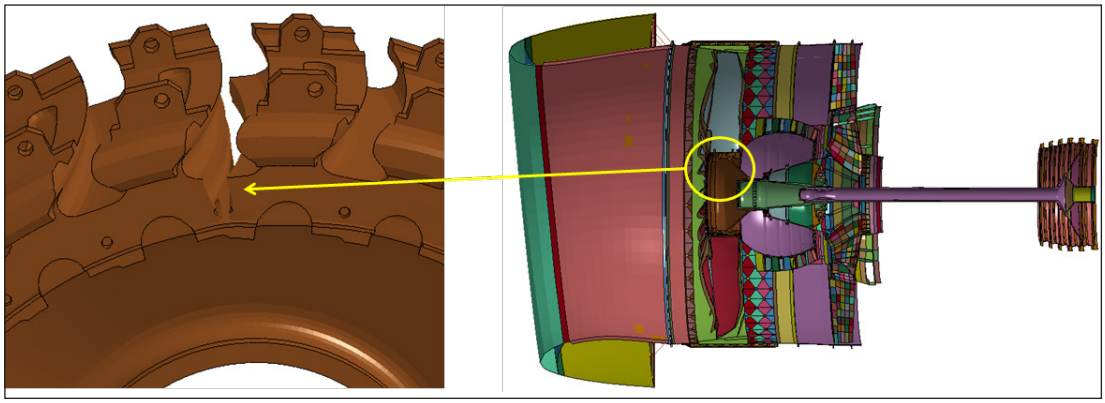

Fig. 2: Hub “bore to rim” fracture scenario simulated by removing hub elements in blade slot

It should be noted that the fan hub “bore to rim” scenario encompasses any scenario that would result in the body of the hub being fractured, as the bore to rim location would be the first to fail in all scenarios.

The simulations showed that the collateral damage and part fragmentation associated with the fan hub bore to rim fracture was consistent with findings on the available hardware, including the fan containment case damage, Kevlar® belt damage, low pressure compressor drum front face scratch patterns, and the condition of the fan blades recovered both from the ground in Greenland and from the engine on the aircraft.

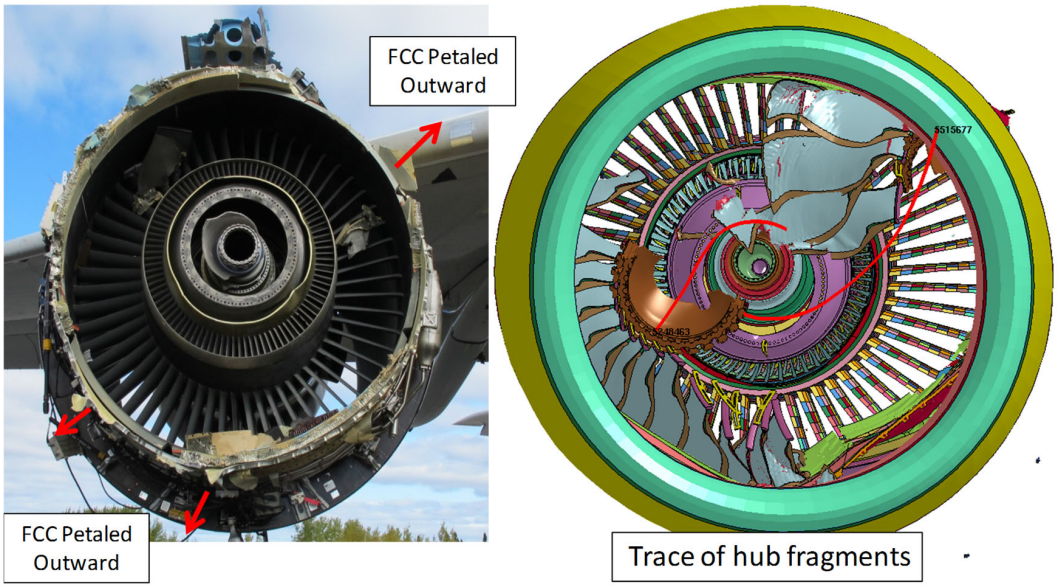

Source: EA

Fig. 3: Simulation of fan hub "bore to rim" failure is consistent with damage observed on event engine

The LS-Dyna simulation was also used to estimate the size, mass, velocity and angle of ejection of each hub fragment, to help refine the ballistic computation and the search area on the Greenlandic ice sheet.

Fig. 4 shows the scenario which was deemed to be the most consistent with the damage observed on the engine (Kevlar® belt, fan containment case, bulkhead damage etc.). It is actually half a revolution of the right hand image of Fig. 3, as the o'clock angular position of the fan hub failure was arbitrarily chosen, and was modified to correspond to the damage observed on engine No.4.

According to the LS-Dyna simulation, a first fragment (later called Fragment 1), weighing 200 lbs (91 kg) exited the fan case at a speed of 435 ft/sec (133 m/s), at an angular position between 4 and 6 o'clock, aft looking forward[5]. A second fragment (Fragment 2), weighing 281 lbs (127 kg) exited the fan case at a speed of 186 ft/s (57 m/s) at an angular position of approximately 11 o'clock.

From the simulation and the manufacturer's experience, all blades were expected to be released from the hub before fragments fall to earth.

From that point, two fan hub fragments were looked for instead of the three initially expected after the phase II calculations. The first fragment was two fifths of the hub, the second, three fifths.

[5] Unless otherwise stated, all angular positions are given aft looking forward.

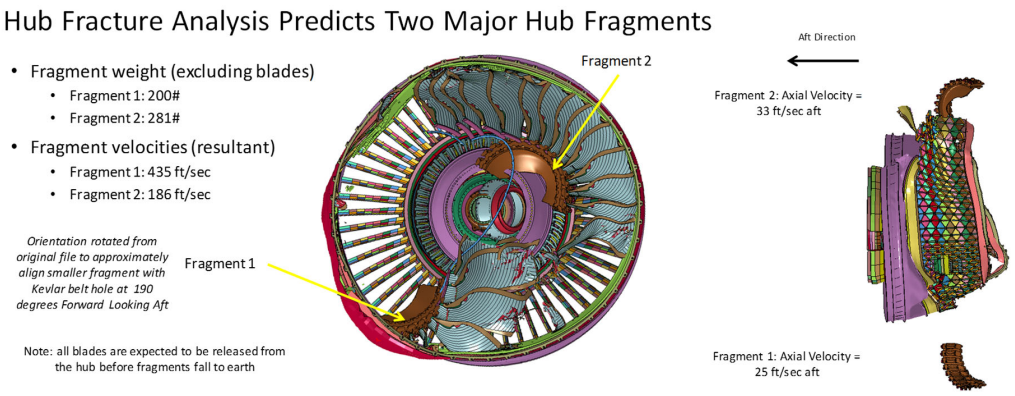

Source: EA

Fig. 4: Simulation results of the fan hub bore to rim rupture scenario, consistent with damage observed on engine

1.2 Ballistic computation updates

1.2.1 Refined data

To support search phases I and II, the NTSB, the BEA and Airbus performed ballistic computations in order to determine the probable area in which the fan hub fragments were located.

These first calculations were performed quite early on in the investigation, and data supporting these calculations were not refined further at that time, due to time constraints.

After search phases I and II, the event flight data were looked at more closely. It became apparent that the initial location of the event used for the computations did not exactly match the aircraft position at the time of the engine failure. The reason for this mismatch could not be determined.

Moreover, thanks to the LS-Dyna simulation, new velocity data for the ejection of the fragments were made available and could possibly refine the search area.

For those reasons, it was decided to consolidate the hypothesis used for the ballistic trajectory computation of the debris, and then to re-launch calculations with these new pieces of information.

1.2.1.1 Aircraft position at time of event

In the FDR data, three sources are available for positioning the aircraft:

- GPS
- IRS (inertial reference system)
- FMS (flight management system), which is a combination of GPS and IRS data.

Initially, the BEA decided to take into account the GPS position parameters from the FDR to determine the event coordinates and to use it as a starting point for the ballistic computations. The IRS data were laterally offset by up to 80 m, at Paris Charles-De-Gaulle airport as well as at Goose Bay airport (see Fig. 5) whereas the GPS position was consistent with both airports.

Amongst the points considered when refining the event coordinates for the next search phase, was the FDR position parameter source to be used. Indeed, even if the GPS data are very accurate in terms of position, Airbus explained that its dating can be less precise as delays can be up to 2.2 seconds due to the GPS position refresh rate of one second, data latency and the FDR recording rate of the parameter. This would give an offset in the aircraft longitudinal position.

The IRS position is spatially accurate during takeoff only, when all systems are initialized correctly. It can show lateral discrepancies during the flight. But it is refreshed every 80 ms.

The FMS position is based on the GPS position and on the IRS position. Given the refresh rate of the IRS position, the FMS position dating can have delays of up to 1.39 seconds.

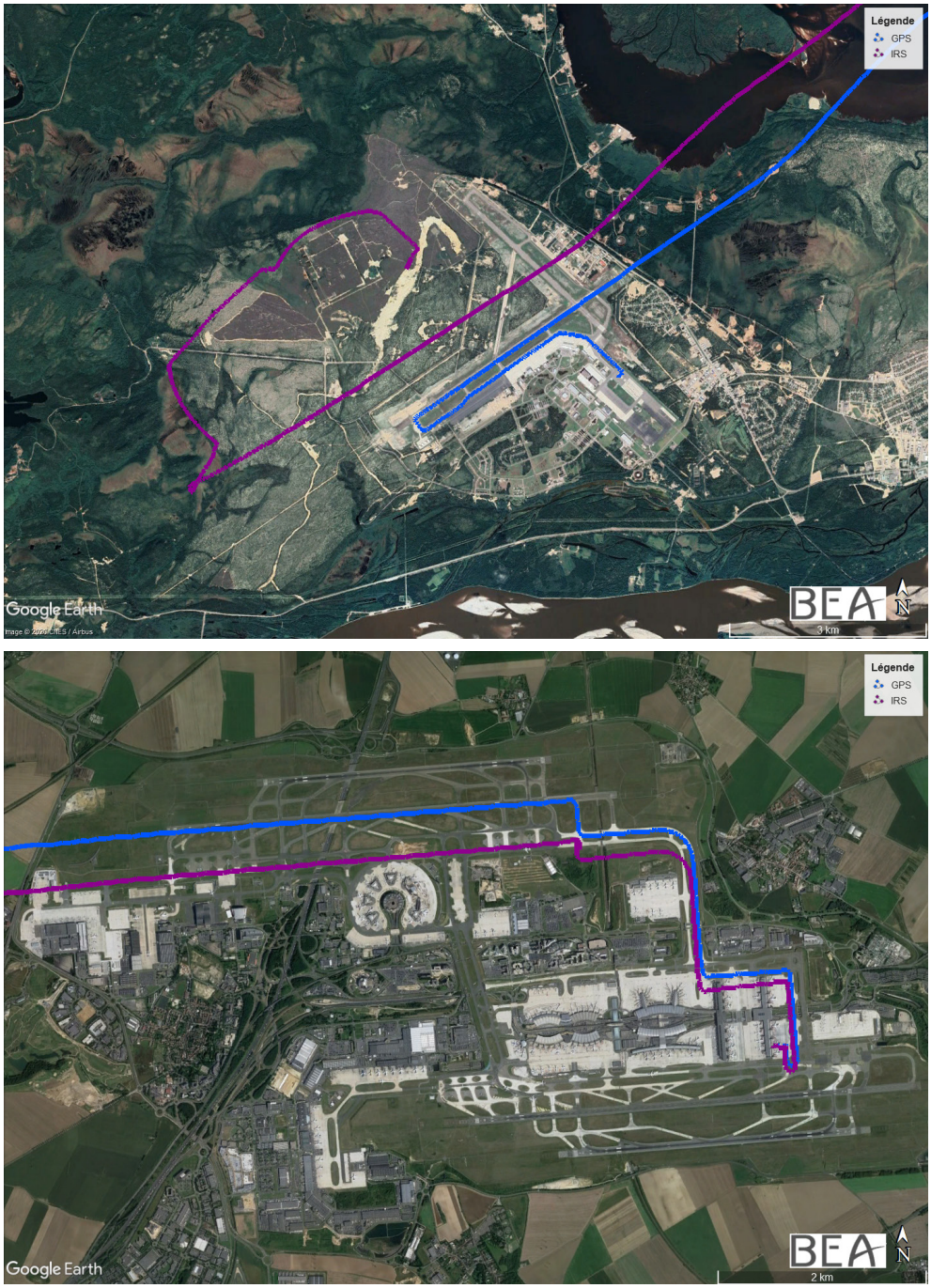

Fig. 5: Comparison between GPS (blue) and IRS (purple) position data at Goose Bay (top) and Paris Charles-De-Gaulle (bottom)

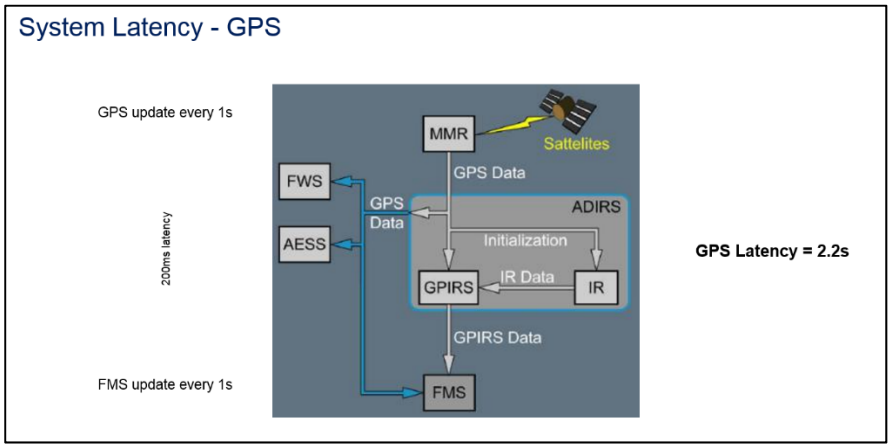

Source: Airbus

Fig. 6: Computation of FMS data from GPS and IRS data

It was jointly decided with Airbus to use the FMS data to locate the event as it uses the spatial location of the GPS, which is more precise, and the shortest dating interval of the IRS. The captain FMS position parameters were finally taken into account to locate the event.

The updated location of the event (light blue point below in Fig. 7) was then:

61.744080°, -46.823104° at 13h49m18.506s[(6)]

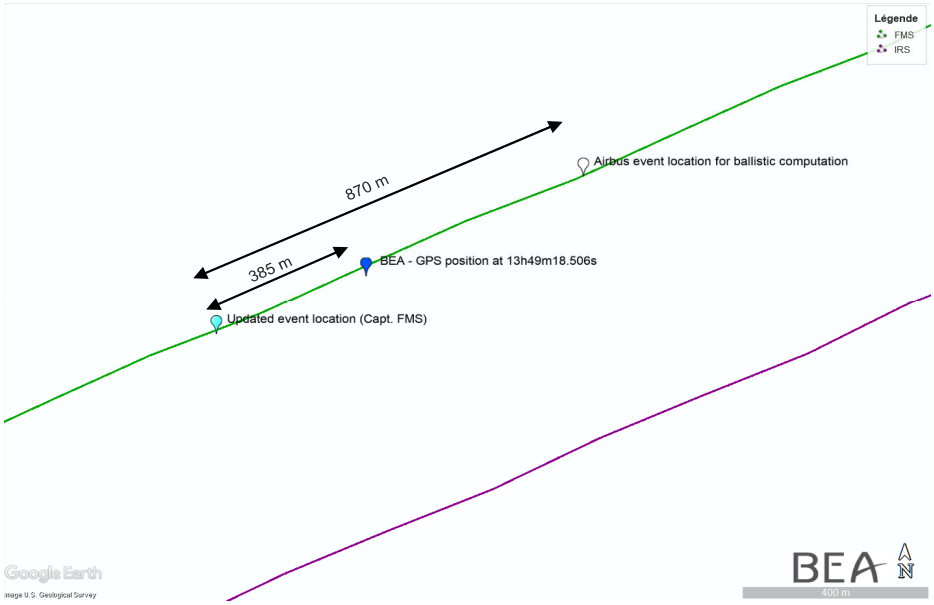

Fig. 7: Comparison of event positions: updated (FMS) location of event (light blue), initial BEA (GPS) event position (dark blue), Airbus position taken into account for Ariane computations (white)
Green line is FMS trajectory, purple line is IRS trajectory

The distance between the updated location of the event (Captain's FMS position, light blue) and the initial BEA (GPS position, navy blue) location of the event was 385 m. The distance between the updated location of the event and the position Ariane used for ballistic computations was 870 m.

[(6)] The event trigger time was the first peak of lateral acceleration, see (BEA, 2019).

1.2.1.2 Aircraft geometric altitude at time of event

Discussions were held about the geometric altitude of the aircraft when the event occurred. Pressure altitude is generally used with reference to Standard Atmosphere (1,013 hPa at sea level) in the en-route phase.

For accurate ballistic computations, the geometric altitude of the aircraft as well as the altitude of the terrain were necessary as input data. In other words, the aircraft elevation above the ground was needed.

Several altitudes were recorded in the FDR data. A comparison of the pressure altitude and GPS altitude was made in order to verify that they were consistent with each other, and to determine the aircraft elevation above ground at the time of the event.

In Fig. 8, the GPS altitude shows some variations during the flight, in the en-route phase in particular, while the flight level (measured in terms of pressure altitude) was constant. The comparison between the two altitudes was not easy.

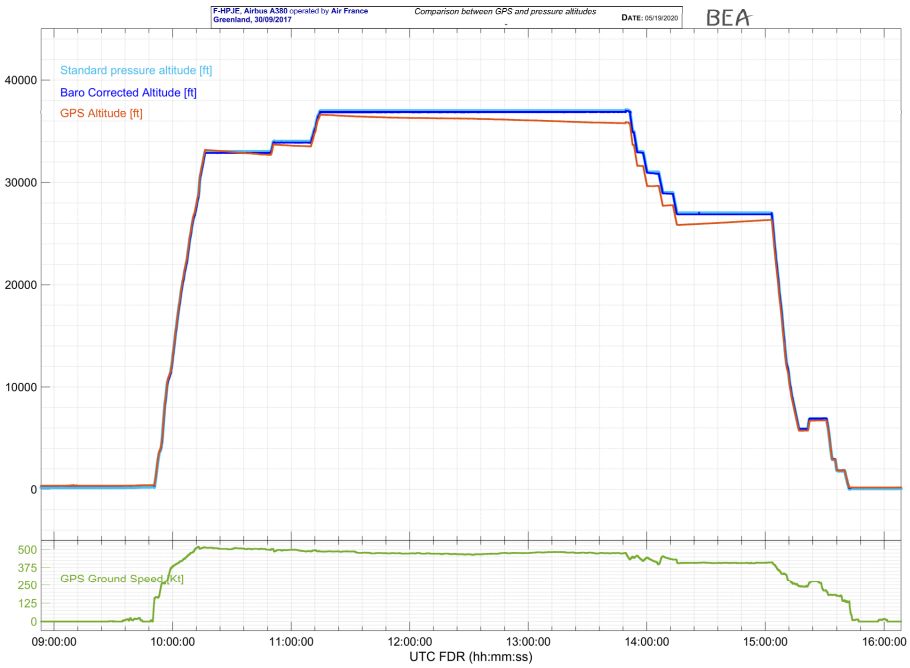

Fig. 8: Comparison between barometric altitude (blue) and GPS altitude (orange)

The GPS altitude corresponds to an altitude above the Earth geoid whereas the pressure altitude indicates the altitude obtained with the measured outside static pressure when the altimeter is set to 1013 hPa, based on the assumption that the atmosphere profile follows the standard atmosphere model. This means that is it necessary to apply QNH and temperature corrections to obtain the geographic altitude from the pressure altitude. Those corrections are made with the hypothesis that the current atmosphere over Greenland follows the same variations as the standard atmosphere. If there is a temperature inversion for example, the corrections are no longer valid.

The static temperature recorded in the FDR indicated differences with the International Standard Atmosphere (ISA), known as Δ_{ISA}, which were not constant along the flight.

GPS altitude

A GNSS specialist contacted by the BEA indicated that above a latitude of 60° (the event was located at approx. N61.7° W46.8°), the GNSS coverage can show some high limitations. These limitations are not due to the fact that the GNSS receiver does not see many satellites, but rather due to there being no satellite strictly at the vertical of the receiver. The accuracy of the available GNSS altitude depends on the receiver, on the number of satellites, if there is any enhanced function in the receiver such as EGNOS (European Geostationary Navigation Overlay Service), and what data is recorded. It is possible to have a gap in the enhanced GNSS function around Greenland.

Pressure Altitude correction

Corrections were applied to the pressure altitude recorded in the FDR in order to compare it with the GPS altitude. The closest airport to the location of the event was Narsarsuaq, code UAK.

On 30 September 2017, the UAK QNH at 01:50 UTC was 995.2 hPa, meaning that a correction of -500 ft had to be applied to the pressure altitude to match the QNH. Even with this correction, the computed barometric altitude was significantly different to the GPS altitude. This meant that some temperature corrections were potentially needed, and the local QNH was potentially different from the one in Narsarsuaq. But the Δ_{ISA} was not constant, and it seemed likely that the atmosphere was not following the standard atmosphere.

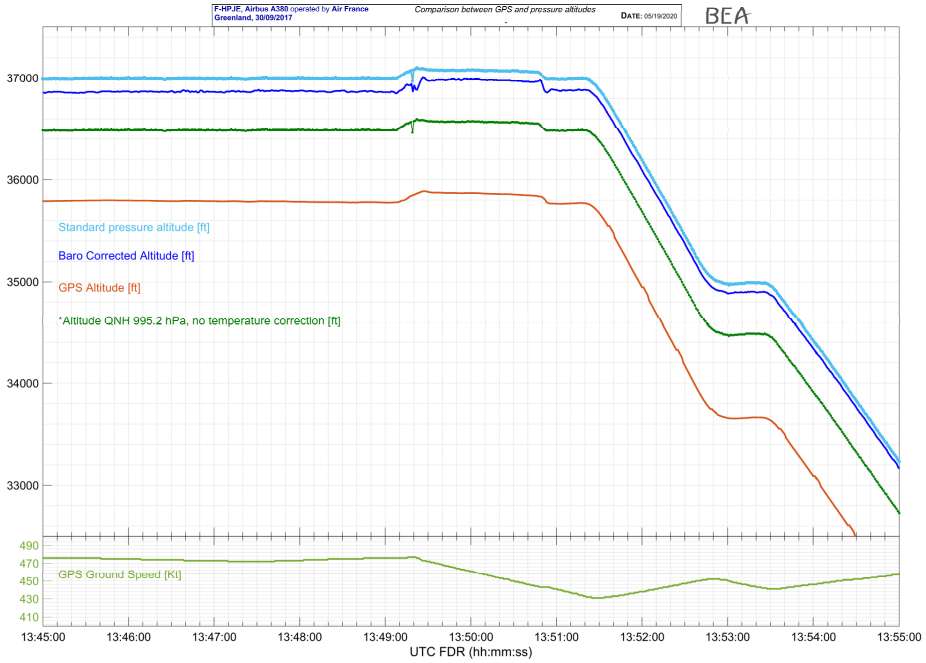

Fig. 9: Altitude data recorded at time of engine failure (13:49:18)

Airbus was asked to evaluate the correction to be applied to the barometric altitude, to obtain the true geometric altitude. Airbus answered that obtaining the geometric altitude from a barometric altitude measurement close to the North Pole was tricky, because the atmosphere profile significantly differs from a standard atmosphere model.

To help determine the geometric altitude, Airbus provided a data export from NOAA (National Oceanic and Atmospheric Administration, USA) in September 2017 (see Fig. 10).

NOAA data was given for a location which is 950 km from the location of the event, and for 12:00 UTC whereas the event occurred at 13:49:18 UTC (see Fig. 10).

Fig. 10 exhibits a temperature inversion at around 30,000 ft. This confirms that applying temperature corrections to a barometric altitude is not straightforward and could be biased as the atmosphere at the location of the event did not follow the standard atmosphere model.

NOAA data gave, for a standard barometric altitude of 37,080 ft:

- a MSL[7] altitude of 35,840 ft at 06:00 UTC
- a MSL altitude of 35,760 ft at 12:00 UTC
- a MSL altitude of 35,720 ft at 18:00 UTC

[7] Mean Sea Level.

The NOAA altitude value of 35,760 ft at 12:00 UTC is consistent with the GPS altitude recorded at the time of the event, **35,840 ft**.

Even if the GPS altitude can show some limitations in northern latitudes, the consistency between the NOAA altitude values and the recorded GPS altitude led to the recorded GPS altitude being chosen as the geometric altitude at the time of the engine failure.

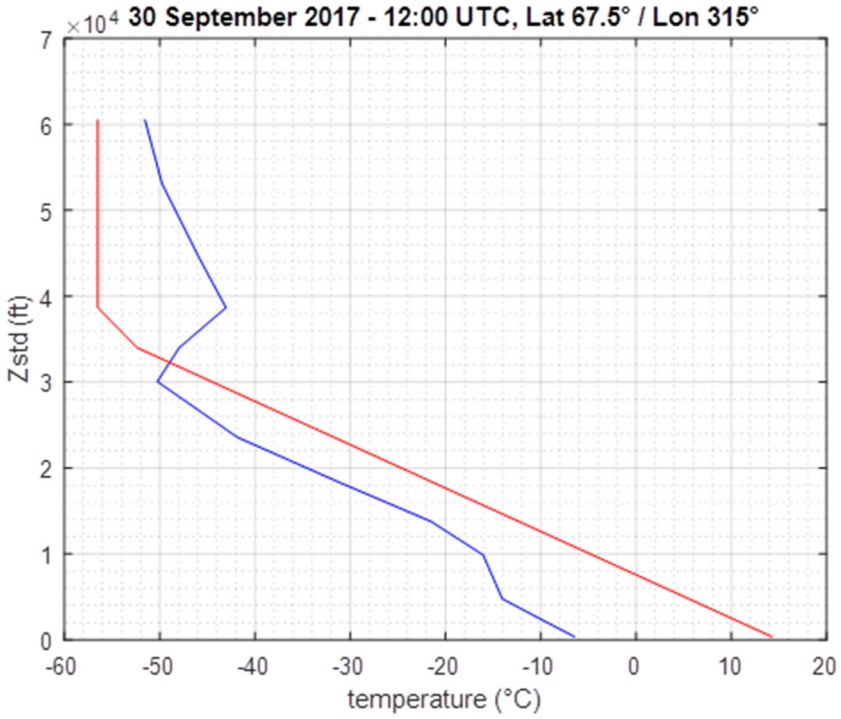

Fig. 10: NOAA data (source Airbus) showing temperature profile versus altitude at 12:00 UTC, 67.5°N, 31.5°W. Red line is standard ISA temperature lapse rate and blue line is reported temperature lapse rate at that date and time

1.2.1.3 Terrain elevation

The terrain elevation in the search zone can show variations of +/- 1 m depending on the snowfalls, the melting periods, the ice movements, etc. It was first estimated by GEUS, using data provided by BedMachine[8], a bed topography and bathymetry map of Greenland, and ArcticDEM[9], a digital elevation model. GEUS confirmed the data once on-site in March 2018 with a hand-held GPS. The mean altitude of the search area was approximatively 6,070 ft MSL (1,850 m). The northeast corner of the debris field was at 1,950 m, whereas the southwest corner of the search area was at 1,800 m.

The values were confirmed by ONERA's post-processing of radar data.

1.2.1.4 Fragment depth

During Phase II, the depth of the fragments under the surface was estimated to range between 2 and 3 m. This included the penetration depth due to the impact of the fragments with the ice sheet surface, and one season of snowfalls. In view of a field campaign in the spring of 2019, in other words one year after Phase II, an additional season of snowfalls had to be taken into consideration to estimate the actual depth of the fragments. Based on the figure of 1 to 1.5 m of snow accumulating during a season, the actual depth of the fragments was thought to range between 3 and 4.5 m.

1.2.2 Ballistic computation updates

1.2.2.1 BEA ballistic calculations

With the initial velocity speed provided by the LS-Dyna simulation and the refined data, the BEA computed new ballistic trajectories for both scenarios (ejection at 5 and 11 o'clock positions) and both debris sizes. The aim was to check the consistency between targets detected by the aerial search and the ballistic computations results. The initial hypotheses for debris sizes and ejection are given in (Table 1).

	Fragment 1	Fragment 2
Weight	91 kg	127 kg
Velocity (Resultant)	133 m/s	57 m/s
Ejection Radial	11 o'clock	5 o'clock
Velocity (Axial (Aft))	7.6 m/s	10 m/s

Table 1: fan hub fragment characteristics at hub failure

Due to the unknowns with respect to the shape of the debris (presence or not of fan blades, real shape of the part, etc.) and to their behavior during the fall (e.g. possibly rotating around itself, presence of Magnus effect), it was decided to only consider areas where there was the highest probability of finding parts.

Taking into account the weight of the hub and its size, an average ratio of 235 kg/m^2 was used for the weight over surface ratio needed to compute ballistic trajectories.

For the drag coefficient, the lower boundary corresponded to an aerodynamic profile (around 0.05), which was certainly too small to be characteristic of the fragments being looked for.

[8] Morlighem, M., C. Williams, E. Rignot, L. An, J. E. Arndt, J. Bamber, G. Catania, N. Chauché, J. A. Dowdeswell, B. Dorschel, I. Fenty, K. Hogan, I. Howat, A. Hubbard, M. Jakobsson, T. M. Jordan, K. K. Kjeldsen, R. Millan, L. Mayer, J. Mouginot, B. Noël, C. O'Cofaigh, S. J. Palmer, S. Rysgaard, H. Seroussi, M. J. Siegert, P. Slabon, F. Straneo, M. R. van den Broeke, W. Weinrebe, M. Wood, and K. Zinglersen. 2017. BedMachine v3: Complete bed topography and ocean bathymetry mapping of Greenland from multi-beam echo sounding combined with mass conservation, Geophysical Research Letters. 44. https://doi.org/10.1002/2017GL074954

[9] Porter, Claire; Morin, Paul; Howat, Ian; Noh, Myoung-Jon; Bates, Brian; Peterman, Kenneth; Keesey, Scott; Schlenk, Matthew; Gardiner, Judith; Tomko, Karen; Willis, Michael; Kelleher, Cole; Cloutier, Michael; Husby, Eric; Foga, Steven; Nakamura, Hitomi; Platson, Melisa; Wethington, Michael, Jr.; Williamson, Cathleen; Bauer, Gregory; Enos, Jeremy; Arnold, Galen; Kramer, William; Becker, Peter; Doshi, Abhijit; D'Souza, Cristelle; Cummens, Pat; Laurier, Fabien; Bojesen, Mikkel, 2018, "ArcticDEM", https://doi.org/10.7910/DVN/OHHUKH, Harvard Dataverse, V1, [Accessed Fall 2017]

Taking into account that a round bar has a drag coefficient of 1.0 while a thin plate has a drag coefficient of 0.78, it was decided to select a drag coefficient of 0.9 for the upper boundary condition.

To deal with the uncertainties described above (presence or not of Magnus effect, weight over surface ratio, drag coefficient, etc.), an error of + or -2% on the flying distance of the part was considered.

Due to software settings, true computations were performed with a weight over surface times drag ratio (W_t/C_DS) between 270 kg/m² and 5,000 kg/m². The areas obtained where objects might have fallen are presented in Fig. 11.

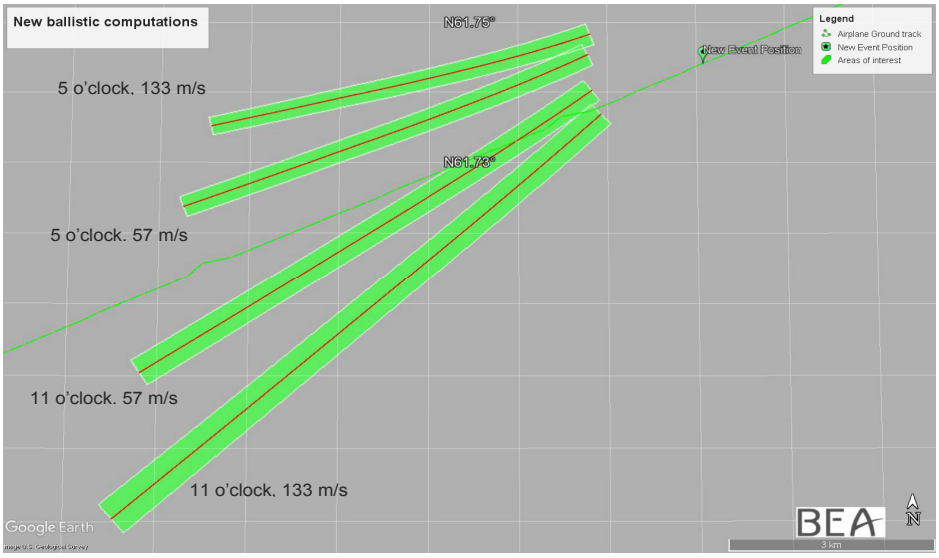

Fig. 11: Locus calculation for the two speeds (57 and 133 m/s) and the two angles of ejection (5 and 11 o'clock) from LS-Dyna simulation

1.2.2.2 NTSB ballistic calculations

The NTSB did a new iteration of ballistic coefficients for the missing fragments, now having initial velocity vectors from the LS-Dyna simulation (see 1.1) and taking into account the refined data (see 1.2.1). Generally, the drag or ballistic coefficient is estimated based on experience with similar parts. The NTSB participated in two drop tests in the early 80's where it calculated ballistic coefficients from measured falling times. In addition, over the years, when the NTSB recovered items of wreckage, their ballistic coefficients could be deduced by comparing their theoretical position on the ballistic ground locus with their real position on the ground.

So taking into consideration the shape of the fragments, the NTSB used a range of ballistic coefficients based on the following calculation:

Fragment 1 was estimated to be 38% of the hub with all of the inner connection to the shaft gone. It would most likely fall with drag between an outside front down stable flat fall and a tumble about its long axis and front first. It is possible that mass distribution along the circumference would be constant so that this part could develop organized lift (i.e. be a flyer).

W_t = 91 kg (200 lbs)
Top Down:
$S^{(10)}$ = 0.38 (2Lπ r)
S = 576.5 in^2 = 4.0 ft^2
C_D = 0.9
Front Down:
S = 0.38(π r^2 - π r^2)
S = 133.8 in^2 = 0.93 ft^2
C_D = 1.1
W_t/C_DS = 201/(0.9 * 4.0) to 201/(1.1*0.93)
W_t/C_DS = 55.83 to 196.5 lb/ft^2

Fragment 2 was estimated to be 62% of the full hub with some of the inner connection to the shaft still attached. It would most likely fall front down at a shallow angle.

W_t = 127 kg (280 lbs)
S = 0.62(π r^2 - π r^2)
S = 0.62 (3.14159) *(17^2 – 13.3^2) = 218.4 in^2 (1.52 ft^2)
C_D = 0.9 to 1.2 with probable angle range (note the 1.2 is actually from increase presented to flow)
W_t/C_DS = 280/(1.2 * 1.52) to 280/(0.9 * 1.52)
W_t/C_DS = 153.5 to 204.7 lb/ft^2

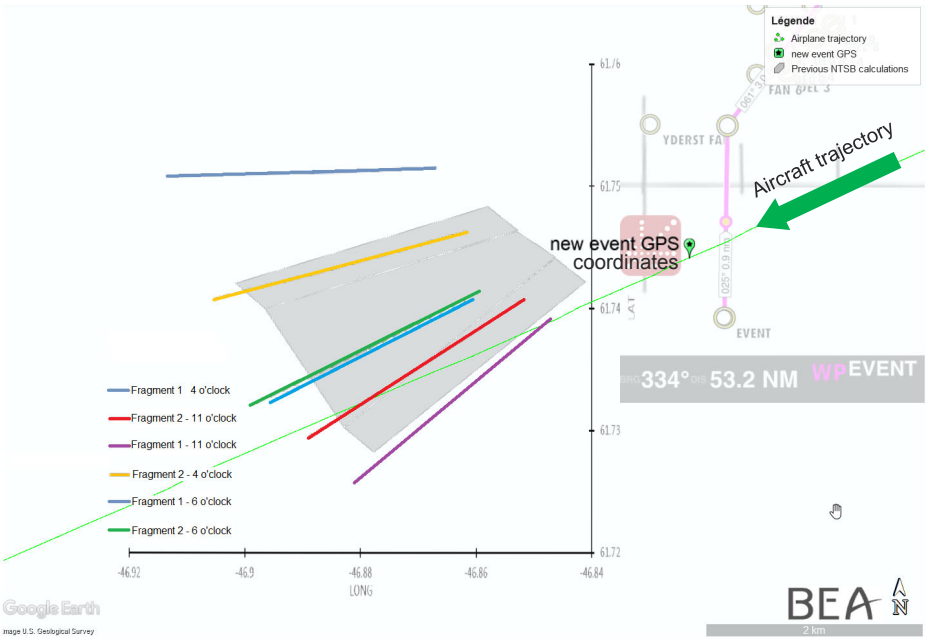

Fig. 12: Locus calculation for the two fragments. Each fragment was simulated leaving the engine with a radial angle vector corresponding to 4, 6 and 11 o'clock. 4 and 6 o'clock were chosen to mark off the probable position of the debris which exit at the 5 o'clock position, as there were uncertainties on the damage observed on the engine. Grey area is previous NTSB search area calculated in early 2018

Fig. 12 shows the updated ballistic computation carried out by the NTSB. The area in grey was the search area obtained with the early 2018 calculations as described in the report in reference (BEA, 2019). Colored segments show the ballistic locus obtained with the new data (updated event location, simulated mass and velocity of fragments, ranges of ballistic coefficients and angles of ejection). The search area was globally shifted west compared to early 2018. Those calculations do not consider any shift due to ice sheet movement.

[10] S is a specific reference area for drag coefficient calculation and that reference area was picked for ease of calculation at the wreckage orientation under consideration

1.2.2.3 Airbus ballistic computations

Several sets of data were available as starting hypothesis regarding the departure of the fragments from the airplane and their fall: damage observations on the engine, LS-Dyna simulation results and recorded flight data. Weight, geometry, speed and angle of ejection of the fragments were estimated from LS-Dyna simulations and engine damage observations. The location of the event along with the altitude and the speed of the aircraft were known from the recorded data. However, the location of the event was updated after Phase II (see paragraph 1.2.1). Therefore, the need to perform new ballistic computations was discussed.

However, it was finally considered unnecessary to conduct these new computations with the Airbus method as the hypothesis used at the time of the first calculations (late 2017) was deemed close enough to final data. The only difference was the location of the event, which shifted approximately 800 m from the aircraft trajectory, as presented in chapter 1.2.1.1.

In late 2017, results were then shifted approximately 800 m. This shift did not take into account any ice sheet movement. The original position of the search areas was however still considered, as a secondary search zone.

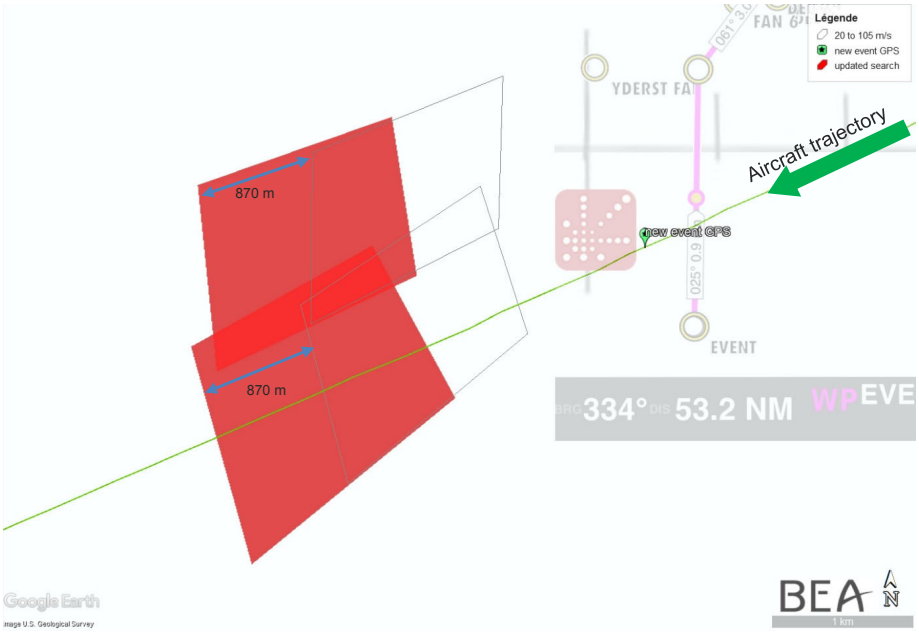

Fig. 13: Shifted search area (in red) based on late 2017 Ariane computations (in grey)

1.2.2.4 Updated search areas

Given the update of the LS-Dyna simulation results, the readjustment of the event location (paragraph 1.2.1) and the slight changes in the ballistic computation results, an update of the search area was proposed for a systematic search, taking into account that its size had to be reasonable enough to be surveyed by systematic ground capabilities during a 4-week field campaign.

As for search Phase II (BEA, 2019), an overlap of the different ballistic results was considered to determine primary and secondary search areas.

The red areas in Fig. 14 are areas where readjusted Airbus results and NTSB ballistic computation results overlapped. It should be noted that the BEA results and the NTSB results were quite similar. The orange areas are areas where only one calculation, either the readjusted Airbus computation or the NTSB ballistic computation predicted the presence of a fragment.

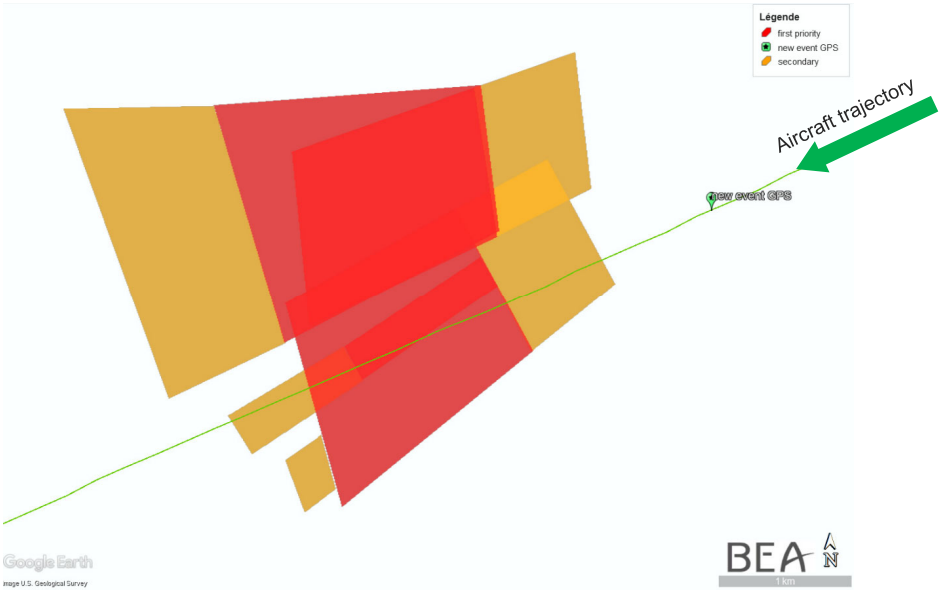

Fig. 14: Updated primary (red) and secondary (orange) search areas

An extended search area was determined, surrounding the red and orange areas (light blue in Fig. 15) to account for input data uncertainties. None of these areas took into account any ice sheet drift: in other words they were valid at the time of the event only.

To take this drift into account, a dilation was applied to the light blue area, as presented in dark blue in Fig. 15. The dilation was approximately 200 m west and 200 m south, and applied to the west and south corners, to remain conservative (it was not applied to the north-east corner).

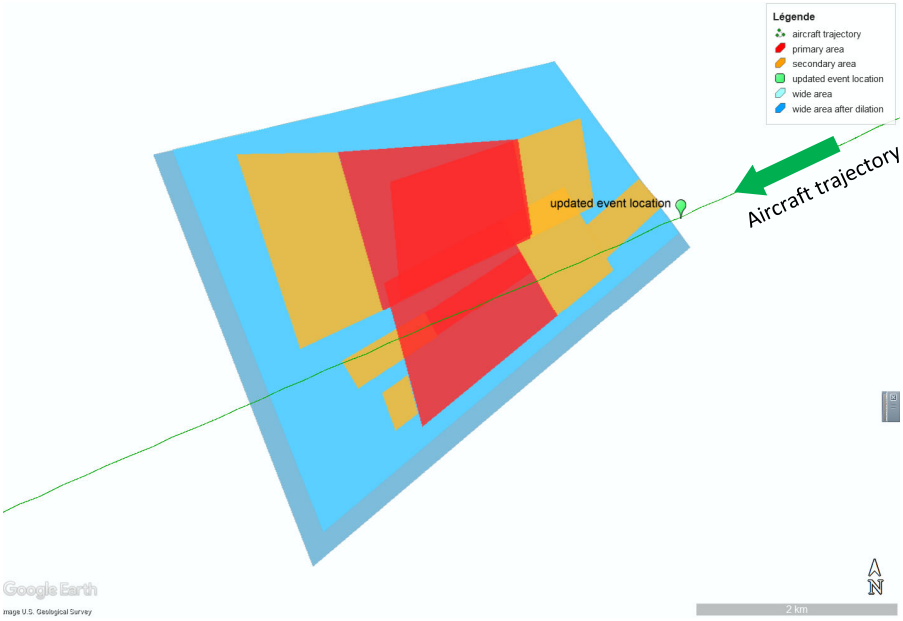

Fig. 15: Final updated search area. Primary (red) area is 4.4 km², secondary (red + orange) is 8.10 km², and wide area after dilation (dark blue) is 17 km²

1.3 Radar imagery data analysis

1.3.1 General

The initial processing of the X, L and UHF band images acquired during the airborne radar image acquisition campaign carried out in April 2018 did not yield any convincing hub fragment detection, because of both the high clutter[(11)] level and the low target cross-section in low frequency bands or the high target echo attenuation in high frequency bands.

However, further post-processing showed that the test fan hub part intentionally buried 1.2 m deep close to the search area could be detected in the X-band but with a very poor target to clutter ratio (the fragment echo was only 10% of the clutter level in the same pixel).

In order to reliably detect the fragments being searched for with a reasonable false alarm rate, speckle fluctuations of the clutter had to be reduced well below the target level, hence the image had to be massively multilooked (typically an equivalent number of at least 100 looks was required, see paragraph 1.3.2). This was possible because several independent looks could be computed for each polar channel of each acquisition, and because the acquisition plan involved several headings and several incidence angles.

Care had to be taken to accurately compensate the antenna pattern, the thermal and system noises, the ambiguities and the geometric deformation inherent in the radar geometry in the final composite image (summing a total of 432 single SAR images). A constant false alarm filter followed by a visual inspection of alarms yielded a list of candidate positions of fan hub fragments (as well as several unrecovered light engine fragments).

The next sections describe the SAR post-processing issues for computing massive multilook images focused below surface in a slowly drifting, high backscattering, non-Lambertian[(12)] environment.

1.3.2 Motivation of massive multilooking

The search area during Phase II was approximately 5 by 5 km wide, and any false alarm investigation had a high cost: just after acquisition, digging at one alarm location required shoveling some two tons of snow. Such an operation in a hostile polar environment at a high altitude (1,850 m) is a very demanding task even for highly trained polar explorers.

SAR is inherently a coherent wave sensor, hence its images are affected by speckle. This means that the pixel intensity on a uniform surface is randomly distributed according to Raleigh's law (the bell shaped curves in Fig. 16, left).

Detecting the fragment in the X-band was a challenge: if the target echo adds 10% to the clutter return, it changes the random distribution of the intensity from the red curve to the green curve in Fig. 16, left. Any detection threshold (dashed line in Fig. 16) in a single image would result in a high probability of non-detection (ND, green hatched area) or a high probability of a false alarm (FA) (red hatched area), or both.

(11) Clutter is a term used for unwanted echoes in electronic systems, particularly in reference to radars. Such echoes are typically returned from ground, sea, rain, animals/insects, chaff and atmospheric turbulences, and can cause serious performance issues with radar systems.

(12) Lambert's law corresponds to the uniform diffusion of the incident radiation on the upper half-space of a surface. This results in an apparent luminosity of a surface varying with the cosine of the incident angle in optical images (and to a cotangent in radar images). Rough surfaces generally scatter radiation according to this law, at least this is the case when far from specular reflection conditions. In a side-looking radar context, the incident angle is typically in the 10° to 80° range in the useful portion of the image, hence the standard procedures for image radiometric correction were designed for the Lambert's law case. The ice sheet, however, behaves in a very different way (in the X-band, the surface luminosity can diverge by more than 4 dB from the Lambert's law) because the radiation is mostly reflected from inside the snow cover (and marginally from its surface) and affected by refraction and attenuation in both directions. An optical image equivalent of an ice-sheet would be an opal, whose iridescent glint is also strongly non-Lambertian accounting for its odd aspect.

The multi-looking technique consists in averaging the intensity between independent measurements which results in a narrower bell shape and hence lower FA or ND probabilities for a threshold chosen between the clutter and clutter + target average levels. This is illustrated in the right image in Fig. 16 with 18 independent measurements (the hatched areas are much smaller).

Space multilooking (averaging of neighbouring pixels) consists in averaging independent neighbouring measurements from the same image, based on groups of pixels all containing clutter and target being compared against groups of pixels containing clutter only. However, due to the small size of the target (less than 4 pixels of 20 cm, since the full hub diameter is around 80 cm), this direction proved ineffective. If more than a dozen neighbouring pixels are averaged, more and more "clutter only" pixels in the average would be included, thus making the distribution value converge once again toward the red curve instead of the green curve with a detrimental effect on FA and ND probabilities. Therefore independent measurements from the same pixel location, but on different independent images, had to be averaged. On a given acquisition in the X-band, two things can be done:

- images from the four polarization channels can be averaged (horizontal and vertical electrical fields are emitted alternately and both are received): this results in an equivalence of 3 independent measurements (because of time reversal symmetry between horizontal transmit/vertical receive versus vertical transmit/horizontal receive. This is called "the reciprocity law"),
- images computed to look slightly fore and aft with respect to the antenna axis can be averaged but this is limited to typically 6 images by the antenna pattern in the X-Band (X-Band antenna beam width).

In conclusion, 24 images equivalent to 18 independent measurements can be obtained from any single acquisition in the X-band (i.e. the "equivalent number of looks", or ENL is 18).

In the fan hub case, the search area was covered by 6.10^8 pixels. If a ND probability of 30% and a FA rate of 10% are considered, this would result in millions of false alarms with 30% odds of missing the real target. Thus it was necessary to average images from all available acquisitions to raise the ENL to more than 100 and reach a FA rate (per pixel) in the 10^{-8} to 10^{-7} range, which is small enough to compensate for the large number of pixels in the search zone.

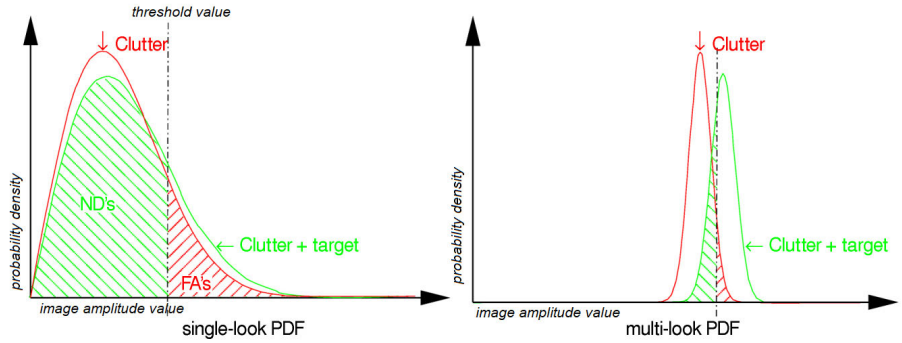

Fig. 16: Comparison of pixel level density function for clutter only in red and clutter + target at 10% clutter level in green for a single look (left) and 18 equivalent looks (right). For a given threshold, non–detections (ND) are represented by the green area and false alarms (FA) by the red area

1.3.3 Technical difficulties for massive multilooking

The possible size of the target on the image was not exactly known: a fragment is a part of an 80 cm diameter hub, and thus may be smaller. The amount of smearing of the target due to blurring by the overlaid snow/ice irregularities was also not exactly known. Therefore, it was decided to compute a full resolution multilook image (i.e. without space averaging) from all available acquisitions in the X-band and add spatial multilooking later on based on the size of the structuring element (SE) for the "top-hat"[13] constant false alarm rate filter (CFAR). Three, five and seven pixels for the SE diameter were tested.

Four headings (parallel & perpendicular to the F-HPJE trajectory) were acquired in the X-band, each heading was acquired as three parallel sub-swathes with a two third overlap between adjacent sub-swathes. Two headings were acquired with a 30° antenna depression. The two others headings (perpendicular to the first ones) were acquired twice (with the InSAR[14] application in mind) with a 50° antenna depression. Thus the total number of acquisition was 18, yielding a grand total of 432 single look images to fuse.

The fusion law for minimizing the speckle is relatively straightforward and depends on the respective signal to noise ratio (SNR). The weight of each component should be proportional to SNR/(SNR+1), with SNR being understood as the "clutter to noise" ratio. The only extra twist here is that the two corresponding cross-pol channels (Hv & Vh) must be incoherently added prior to combining, yielding a 3dB SNR increase.

Besides the computer issues of synthesizing, mapping the images to ground coordinates (images are initially referenced with "slant range coordinates" linked to the radar) and storing 432 images and ancillary data of 25,000×25,000 pixels each, the main difficulties arose from the registration of the images (acquired with different heading and geometry) and the SNR evaluation.

1.3.4 (Absolute) image registration issues

First, tie-points could not be relied on to register images from distinct acquisitions, because the search area was extremely homogeneous, and the calibrator that was set up for that purpose at the edge of the search zone two weeks prior to the ONERA campaign by a GEUS polar expedition (a zenith looking Luneburg sphere) ended up covered with snow in the middle of the ONERA campaign.

Fortunately, ONERA's dGPS hybridized inertial navigation unit (INU) provided a trajectory of high accuracy (10 cm horizontal and 20 cm vertical nominally) which allowed a 10 cm azimuth resolution at a 5 km range without any autofocus. Since there was a reinjection of the transmitted pulse recorded together with the radar signal (and also a "noise" window), the possible drift of the radar internal delays could be calibrated to a fraction of nanoseconds. This results in an absolute image registration accuracy of 50 cm without any tie-point.

Of course, this assumes that the terrain altitude is known. In our context, the digital elevation model (DEM) for the surface was obtained from ICESat[15]. The DEM was locally debiased by a few accurate surface GPS measurements carried out during the GEUS setup expedition and by several vertical SAR surface altimetric profiles.

[13] Top-hat filter refers to several real-space or Fourier space filtering techniques. The name top-hat originates from the shape of the filter, which is a rectangle function, when viewed in the domain in which the filter is constructed.

[14] Interferometric synthetic aperture radar.

[15] ICEsat DEM were provided by the Polar Geospatial Centre under NSF OPP awards 1043681, 1559691 & 1542736

However, the targets being searched for were not at the surface, but buried under 2 to 3 m of snow and ice with an unknown refractive index (but typically 1.25 to 1.35 in the first few meters). So even if the terrain altitude was well known, the exact distance between the radar transmitter and the target was not precisely known. As the SAR side-looks at the target, the vertical uncertainty generated uncertainties when it came to the latitude-longitude position of the target.

1.3.5 Registration depth issues

The actual hub fragment depth was unknown during the radar data post-processing. However, several other engine fragments were detected during this process, some of which were spotted on the ice sheet during the Phase I survey, but not recovered. Given the thickness of the snow layer which had built up between Phase I and the SAR acquisition campaign, it was established that the depth of the hub fragment was certainly between 0 to 1 m deeper than the other observed fragments, i.e. 1 to 2 m below the ice sheet surface at the time of the SAR acquisition.

A numerical simulation with modelling of the overlaid layer as a constant index homogeneous media showed that for the 30° antenna depression geometry, the effect of refraction on a target corresponded, within one pixel, to an offset in altitude (apparent depth) in a media of an index of 1. Hence for these acquisitions, the "apparent" depth could be measured (stereo measurement) when matching salient fragments from opposite headings, and the images registered biasing the DEM with the apparent depth.

For the 50° antenna depression geometry, the incidence angle varied more within the swath, yielding at the swath edges both a vertical offset of the "apparent depth" and a horizontal offset which was slightly higher than a pixel. However, this occurred at the edge of the swath, where the antenna illumination is low with a steeper incidence (with a steeper incidence, the antenna pattern yields a narrower footprint). Hence it was assumed that the corresponding image weight would be very small and the impact of the slightly out of bounds horizontal offset on the overall target smearing could be neglected.

In conclusion, two "apparent depths" were measured for each of the two antenna depression values on salient known fragments and were used to register all images.

1.3.6 Surface motion issue

The images in the X-band were acquired during two flights made five days apart during Phase II, in April 2018. The slow ice-sheet drift towards the ocean, approximately 60 m per year in average according to space measurements, would correspond to a significant 4 pixel mismatch.

The comparison of calibrating target positions measured at setup with the positions measured 13 and 18 days later from the ONERA SAR images were consistent with the large scale values, but showed a higher than expected gradient of longitudinal ice drift velocity (60 m/yr at the test hub fragment burial point, but 100 m/yr at the Luneburg lens location). This high gradient was corroborated by the dense North/South crevasse mesh, probably shear fractures as the difference in velocity exceeds the ice plasticity limit (~2.10^{-2} /yr).

For the multilooking, the second flight was just offset by the average measured drift, the remaining deviation from this average amounting to about 1 pixel at most.

1.3.7 SNR (noise & clutter) evaluation issues

Once geometrically registered, the optimal combination of single-look images depends on the SNR. The accurate evaluation of the SNR requires both a good evaluation of the noise level (mainly thermal noise) and of the clutter level. For this Greenland signal reprocessing, the SAR processor was updated to provide an extra ancillary output which is the thermal noise on the image computed from the noise power density function (noise PDF) for the raw input signal and the actual processing from the raw signal to the final result image (including band equalization, antenna pattern compensation, processing gain, etc.). The noise PDF itself was computed from noise samples measured after each transmitted pulse in a short receive window before the start of the nadir echo (since the ice-sheet is approximately flat, the first echo received by the radar comes from the nadir which is the point just below the aircraft i.e. the closest point at the surface. Before the nadir echo, the only echo from any point of the surface is thermal noise).

The clutter level is critical both for optimal weighting of images with varied SNR, and for normalizing the clutter variations with incidence angle that otherwise induce level discontinuities at the edges of the individual images in the final multilook image (Fig. 17).

The clutter level variation with incidence was modelled for each polarization by adjusting a second degree curve to a level versus incidence angle scatter plot.

This clutter model was used for combining all 432 images into a search composite. Four partial composites corresponding to each acquisition heading were also computed for further target depth assessment.

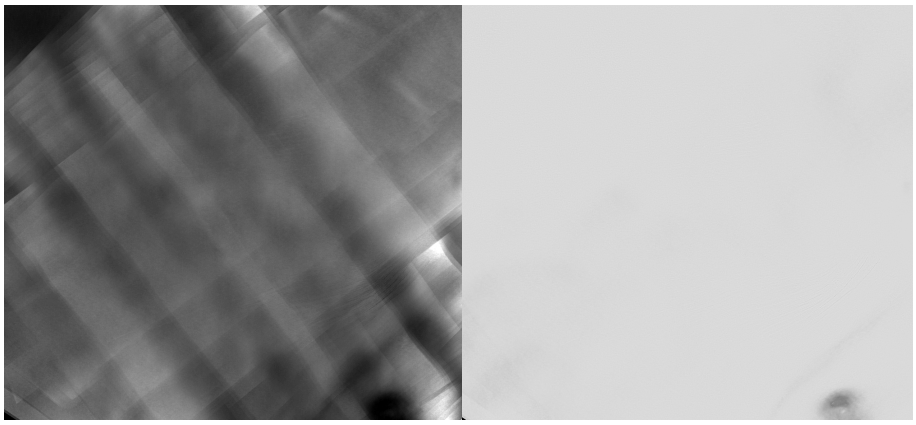

Fig. 17: 432 looks in X-band composite image assuming Lambertian clutter (left with contrast enhanced for emphasis of sub-swathes/look edge discontinuities), and assuming a clutter model deviating from Lambert's law as a degree 2 polynomial function of incident angle (right)

1.3.8 Results

Target detection was performed by a "top-hat" CFAR filter on the final composite image, with a threshold slightly below the level measured on the fan hub test part buried by the GEUS expedition. Filter SE diameters of three, five and seven pixels were tested to accommodate the uncertainties on both the actual target (fragment) size and the target image blur due to ice cover heterogeneity.

This yielded a hundred target candidates, which were each individually examined: first, alarms that appeared just on a crevasse lip were discarded. This was not as straightforward as it may seem, because depending on the position in the search area, the depth of the crevasse lips may differ significantly from the focus depth (the "snow bridge" above the crevasse may be thicker or thinner than the focus depth). Depth difference may cause the crevasse lips to overlay the target position. Here, the visibility of the target from different headings and the comparison with crevasse lip positions made it possible to keep target candidates close to but not at crevasse lips. This point proved important: the recovered hub fragment was just 1 m from the side of a crevasse with the snow bridge ending just 2 m below it (a configuration that made the recovery challenging – see paragraph 4)

Second, targets with position variations between the headings which were not consistent with the expected target depth were also discarded (Fig. 18).

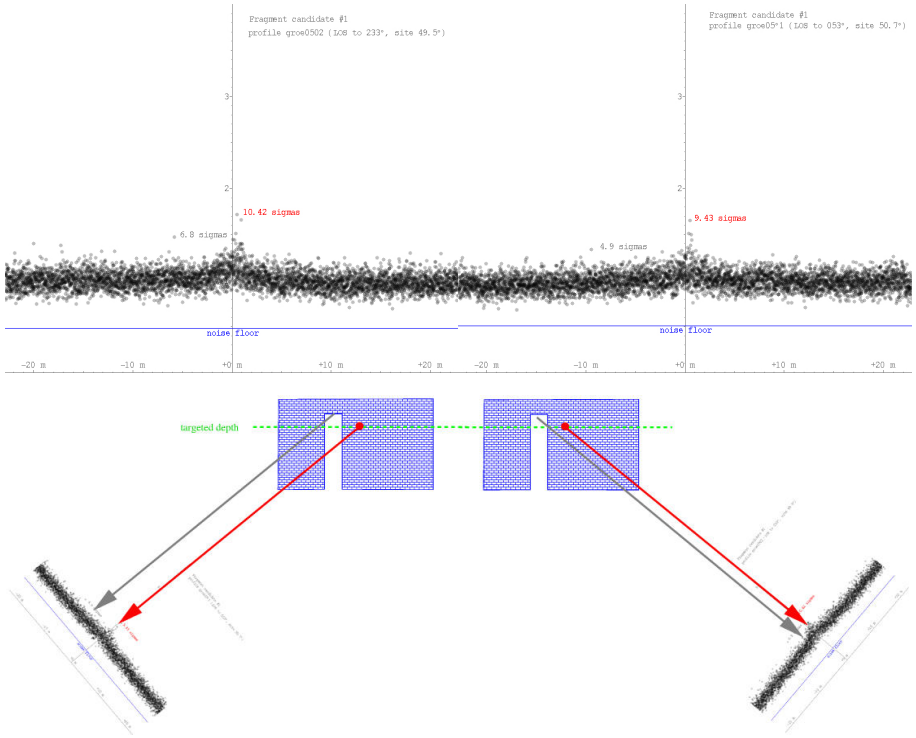

Fig. 18: Comparison of candidate #1 X-band profiles from opposed headings (233°, upper left hand side, 053°, upper right hand side. When comparing profiles of sub-images obtained from opposite imaging directions, the peak of intensity should match if the object is at the targeted depth (red dot, lower image). Features not at the targeted depth (here the low of intensity due to the crevasse air) do not match (grey arrows) because of perspective

1.3.8.1 Results in X-band: hub fragment detection

At the end of the post-processing (with all corrections applied as described above), only one candidate remained (Fig. 19). Due to its position in a dense crevasse field, and because at least two hub fragments were being looked for, "spare" candidates were also identified by relaxing the criteria by lowering the filter threshold.

The GEUS expedition of May 2018 exhaustively scanned (for a period of 3 weeks) some 5% of the search area with the GPR without finding anything. It was assumed that any alarm obtained during the post-processing which was within that 5% was certainly a false alarm. For this reason, the filter threshold in the post-processing was adjusted to just above the first false alarm in the 5% area.

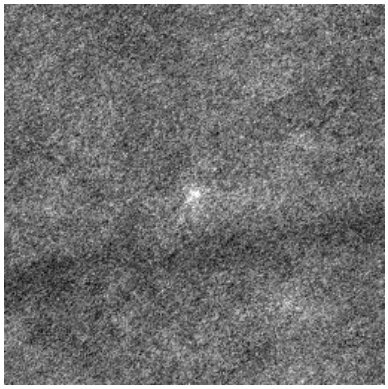

Fig. 19: Candidate (bright pixels) for fan hub fragment on the final X-band image with contrast enhancement for printing. The dark horizontal line is a crevasse under a 6 m snow bridge

The WGS 84 coordinates of the resulting candidate targets, dated 6 April 2018 (i.e. without taking into account any further ice sheet drift), were the following (see Fig. 20):

#1: 46.85348° W, 61.73563° N
#2a: 46.89025° W, 61.75220° N
#2b: 46.85370° W, 61.75392° N

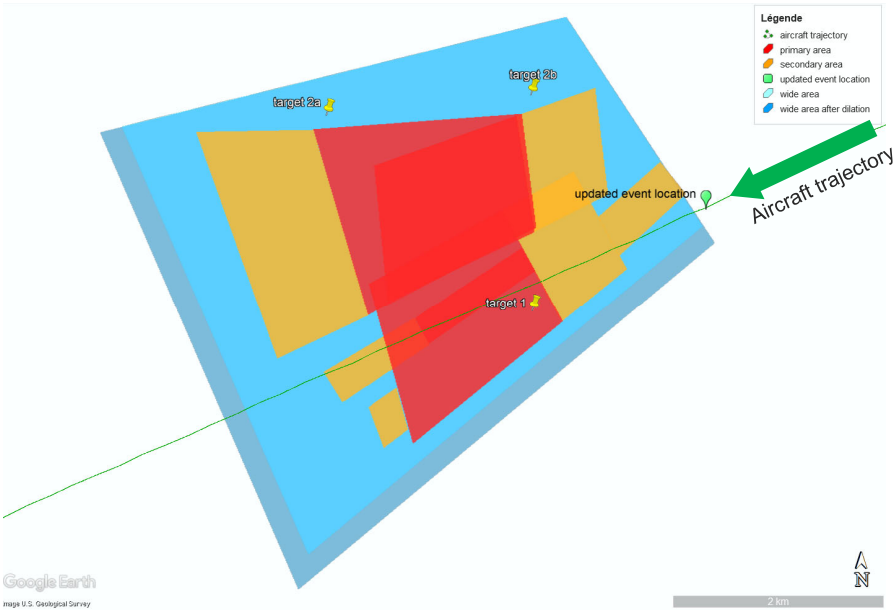

Fig. 20: Location of ONERA candidates 1, 2a and 2b with respect to search area

1.3.8.2 Results in L & UHF bands

During the preparation of the recovery expedition and the expedition itself, the L and UHF-band signals were also reprocessed by ONERA using the same approach as for the X-band described above.

The contrast of the L-band result was too low to effectively detect targets. However, the three candidates obtained in the X-bands could be evaluated: the main candidate was visible in the L-band, but neither of the two "spare" candidates were visible.

Reprocessing in the UHF-band had not been completed when the field campaign was carried out, but partial results were not very encouraging for detecting hub fragments (salient fragments were not or very weakly visible). However, UHF measurements proved critical for the recovery of the hub fragment: due to deeper penetration, crevasses were much more effectively detected in the UHF-band. The comprehensive map of crevasses derived from UHF images (Fig. 21) allowed the helicopter to plan its landing in the safe terrain between crevasses for the installation of the recovery camp and helped the recovery team anticipate the safety issues during the final search and excavation phases.

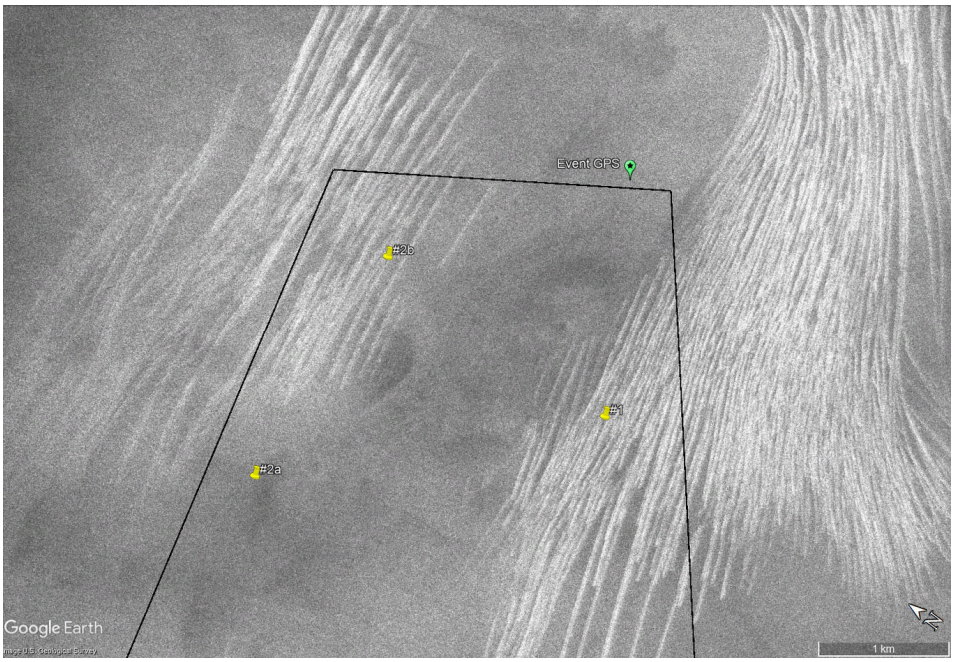

Fig. 21: Example of UHF-band image (vertical polarization) emphasizing the crevasses in the search zone (delimited by black line). Locations of ONERA candidates are marked by yellow plots

1.4 Optical satellite imagery

In preparation for the next potential field campaign and following ONERA's promising results, it was deemed necessary to take a new look at Pleiades images of the search area. Two objectives were pursued:

- knowing ONERA's most promising target position, it was interesting to look at the images from immediately after the event again, to see if the part could be visually spotted and to confirm its location,

- GEUS changed the buried test hub location during the phase II field campaign (Camp Recovery) for calibration and testing purposes; at the end of the campaign, its position was flagged with bamboo poles before they left the site. Two groups of bamboo poles indicated the test hub location, which was right between them. It was good to know if the bamboo poles were still visible from space in order to recover easily the test hub and to estimate the glacier drift between phase II and phase III.

Pleiades images are satellite optical images with a resolution of up to 50 cm. Usable images need a clear sky above the region of interest, see (BEA, 2019) for more information.

Three sets of images were considered: the first one was a set of images dated immediately after the event, when the first clear sky made it possible to have usable images and to see the ground. Those were acquired on 11 October 2017. The second set of data was acquired on 18 May, during the first Camp Recovery field campaign (CR1), and on 28 May (just after it) 2018. The last set was acquired on 17, 19, 21 and 26 April 2019, one year after CR1 and just before the second field campaign (Camp Recovery 2, CR2).

The first set of images was the closest to the event day, which means that if a part was still at the surface at that time, it could have been visible on these images.

When looking at the set of images from May 2018, a mismatch between the coordinates of the satellite images and the real coordinates was detected (Fig. 22) when looking at the two groups of flags left on the camp to mark the buried test hub location.

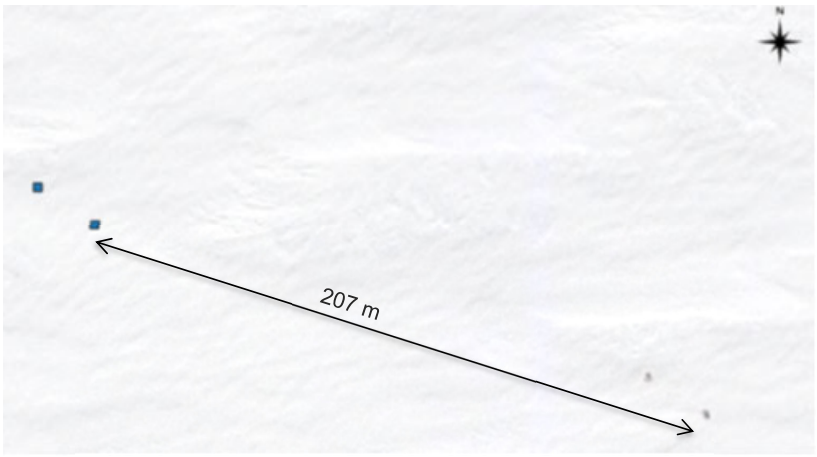

Fig. 22: Pleiades images dated 28 May 2018 – flags are visible from space (two gray dots in lower right). A mismatch of 207 m is observed between real location of flags (blue squares, position recorded in the field via GPS) and satellite image position

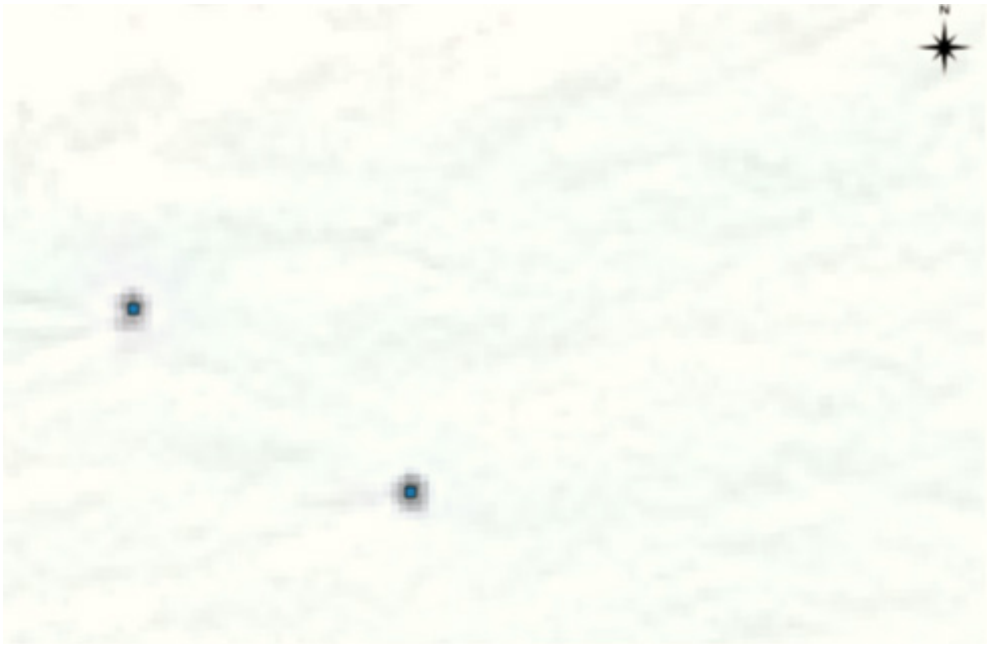

Fig. 23: Pleiades images dated 18 May 2018.
No mismatch is observed between real location of flags as recorded in the field via GPS (blue dots) and flag location in satellite image (gray patches)

The mismatch was not visible on the 18 May images (Fig. 23) when looking at these flags only. However, when looking at the camp location, a mismatch between the camp's real location and the satellite images appeared on both images (Fig. 24 & Fig. 25). The mismatch was of more than 100 m.

The explanation obtained from Airbus was that there were not enough stationary visible patterns (such as rivers, coastlines, lakes) on the images to correctly reference the images to earth coordinates. It was therefore not possible to get accurate GPS coordinates of anything visible on these satellite images.

Despite this issue, the image from 11 October 2017 was looked at again, focusing on the area around ONERA's most promising target. However, no feature could be visually detected on this image (Fig. 26). Indeed it was taken after a few days of cloud cover. Snowfall during these days meant that anything on the surface was no longer visible.

Finally, images from April 2019 were looked at to find the flags marking the buried test hub. No flag was visible anymore, meaning they were buried under snow or blown away by the wind.

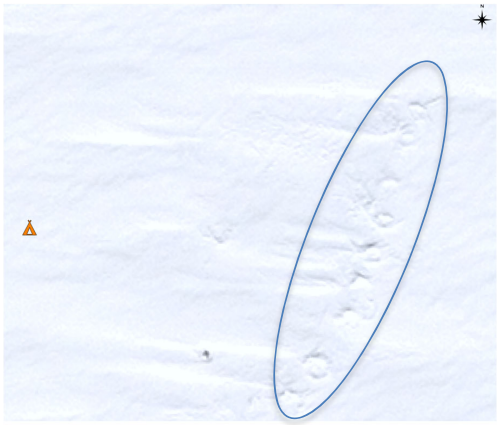

Fig. 24: Pleiades images dated 28 May 2018. Expected camp location marked with orange tent. Traces in the snow (blue oval) indicate the actual tent locations

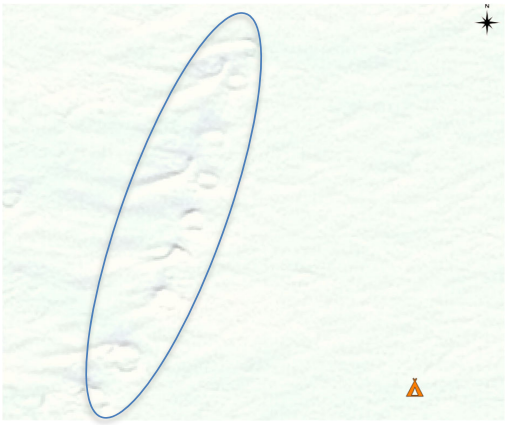

Fig. 25: Pleiades images dated 18 May 2018. Expected camp location marked with orange tent. Traces in the snow (blue oval) indicate the actual tent locations

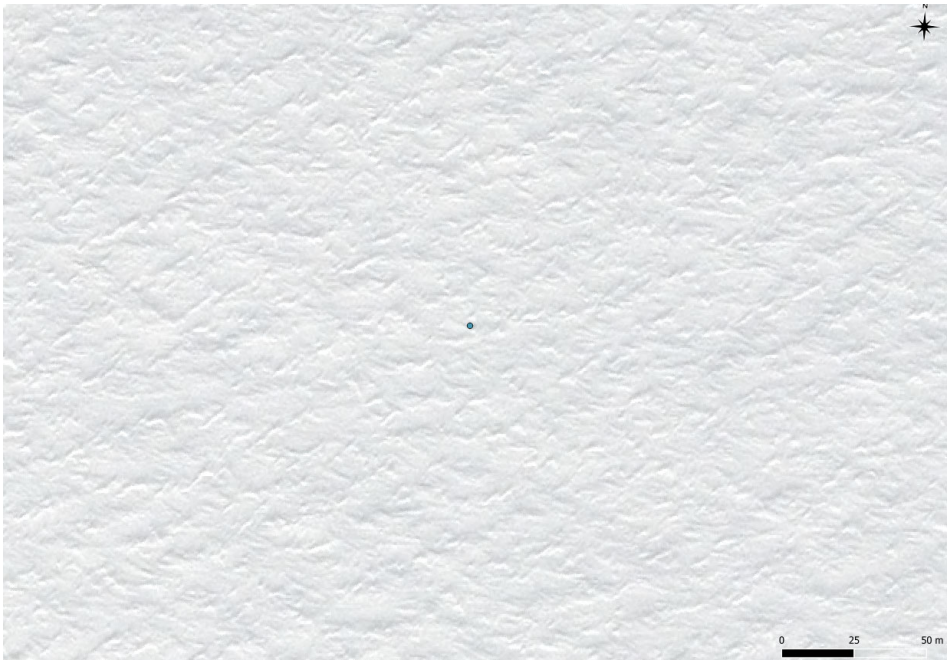

Fig. 26: most promising ONERA target location (blue dot) with background from Pleiades satellite image dated 11 October 2017. No part hub could be observed on the image in this area

2 - EVALUATION OF NEW DETECTION CAPABILITIES

One of the conclusions of search Phase II was that the "GPR had many false positive and false negative results and a small footprint making it a sub-optimal instrument choice for a wide area search" (Mankoff, et al., 2020). Mankoff added that it would be an acceptable instrument if the search area was small and multiple direction crossings could be acquired - that is, for search point targets.

Moreover, even if the test hub was correctly detected on the radar images at the end of Phase II, the risk of having no new high-confidence ONERA target had to be considered.

For these reasons, if there was to be a new, wide-area ground search, more effective detection sensors with a bigger swath and giving a more robust response were needed to launch Phase III.

Several new options for more effective detection were then considered as detailed below. Interest focused on systems for detecting avalanche victims, sniffer dogs and electro-magnetic sensors.

2.1 RECCO

The RECCO system[16] is a commercial, off-the-shelf, mature device which is used for avalanche search and rescue and is available in both helicopter and hand-held versions.

[16] http://recco.com/

RECCO reflectors are lightweight passive transponders which require no power or activation to function. They consist of a diode and an antenna. RECCO reflectors are integrated in products from more than 150 brands, including jackets, pants, helmets, backpacks, back protectors, boots, transceivers, watches and harnesses. Reflectors are also available as single products designed to be attached to helmets and backpacks.

The RECCO detector emits a directional radar signal. When the radar signal hits the RECCO reflector, it is echoed back to the detector and points the rescuer in the direction of the reflector. The closer the detector gets to the reflector, the stronger the returned-signal, ultimately allowing the operator to pinpoint the reflector's location.

The hand-held detector can locate RECCO reflectors within a range of up to 80 m through air and 20 m through packed snow, which results in a practical range of 30 m on avalanche debris.

The RECCO helicopter detector can cover large areas fast. Searching from a height of 100 m and covering a search area approximately 100 m wide, it enables rescuers to search 1 km^2 within six minutes.

The unknown here was that nobody was certain how the system would behave with non-RECCO devices. Moreover, it could not be customized or improved for the purpose of detecting a titanium part. Nevertheless a test was easy and quick to organize.

A RECCO test was therefore performed at the manufacturer's in Sweden, in September 2018, with a test hub fragment.

The titanium test hub did return a signal but only when the hand-held emitter/detector and the fan hub were in one specific orientation. Furthermore, this signal occurred only because the emitted signal bounced off the fan hub, then metal on the operator's jacket, and then to the receiver which then alerted the operator that an object had been detected. This secondary effect, using the operator or a snowmobile is an acceptable mode of operation, but we could not rely on that same orientation in the field with the real fan hub.

When using the RECCO detector with non-RECCO objects, it works best when multiple metals exist and are in contact with each other (for example, electronic equipment with multi-metal circuit boards, or keys on a key chain). Given that the final fan hub, once recovered, contained several metals other than titanium, it is possible that a hand-held RECCO device would be an excellent sensor for this type of search; it is a hand-held, light-weight, affordable, off-the-shelf part with a detection range, field-of-view, and feedback mechanism ideally suited to wide-area ground searches.

2.2 Sniffer dogs

Dogs have a superior olfactory sense to humans and can detect small amounts of odor. Sniffer dogs are dogs which are trained to search for buried bodies and items, by smelling "changes" caused by as little as a few parts per million of odorous molecules. The items can be as various as explosives, illegal drugs, wildlife scat, money, blood, organic fluids such as fuel or oil, or contraband electronics such as illicit mobile phones. Sniffer dogs are also used to search for avalanche victims.

According to the Danish Police, when an object penetrates the ground surface and until it comes to a stop in the ground, it causes a disturbance along its path leading to a higher concentration of oxygen (in small air pockets) than what is present in the surroundings. This can start a degradation process of materials in the soil (snow for example) which gives rise to a scent. It is actually the local increase in oxygen concentration which indirectly creates a scent that the dogs can detect as the greater the amount of oxygen, the higher the possible degradation process, and thus the stronger the scent for the dog to detect.

In 2006, a Beechcraft Baron BE58, registered G-BXNG, made a controlled flight into terrain onto the ice sheet in Greenland, following an engine failure and the impossibility to feather the propeller. The AIB DK issued a safety investigation report relative to this non-fatal accident[17]. The wreckage as well as an emptied fuel barrel which was used for the rescue of the pilot by helicopter at that time were left on site.

[17] https://en.havarikommissionen.dk/aviation-archive/2006/06-510-255/

Late 2017, the Danish police responded to what was most likely an emergency locator transmitter (ELT) signal from the ice sheet.

They dispatched by helicopter with sniffer dogs to the location. Two dogs were led by two police officers. The dogs twice marked for buried objects. They had been given specialized training in buried objects, meaning that they react to smells in areas that are "disturbed" by digging, or by a fallen object or something rotting, etc.

The location matched with the now snow-buried Baron and an abandoned empty fuel barrel (taking ice drift into account) and initial digging for extraction was attempted, but due to lack of resources the digging stopped one meter below the surface, and the ELT stopped after a short while.

It was deemed most likely that the battery giving a low power status message caused the ELT to activate.

Source: AIB-DK

Fig. 27: Sniffer dog before (left) and after (right) dispatch on the ice sheet

While considering the use of sniffer dogs to locate the fan hub fragments, discussions with the Danish police led to the following planned methodology: dogs would have to be trained to work in winter conditions; they would do search patterns in an "S" shape along a line covering 15 x 100 m^2 per hour and per dog. The precision of the markings would be 2 x 2 m^2, based on previous experience. The effective search time would be limited to three hours per day at the location of the event.

Another requirement was a heated shelter for the dogs which had to be used every hour (this could be the helicopter, a heated tent, a heated container). The campaign would be based on in-and-out helicopter transportations, or on a heated camp on site.

Given the surface area that can be surveyed by one dog, four dogs could survey an area of 0.18 km2 in 10 days. As the minimal size of a systematic search area was estimated to be 5 km^2, the sniffer dog solution was discarded.

2.3 Electro-Magnetic (EM) sensors

EM sensors were considered for search Phase II, see (BEA, 2019), and discarded because test results were deemed insufficient at that time. GPR were expected to be more effective, but appeared to be not optimal for a systematic search. Therefore, the EM technology was reconsidered for Phase III.

Scientists from the HydroGeophysics Group of Aarhus University, Denmark (HGG[18]) developed tTEM (a towed transient electro-magnetic sensor), a ground-based method for transient electromagnetic data acquisition, to cover the depth range from 0 to 30 m in full 3D. This extensive section of subsurface is not covered by any other cost effective geophysical method. In reality, the system can "see" deeper than this, up to more than 70 m with a distance between soundings of 3 to 4 m. Typical operating distances between lines are 10 to 20 m resulting in a full 3D "image" of the subsurface.

[18] http://hgg.au.dk/

The system as it existed initially was quick to deploy and easily manageable by a field crew of two persons. It consisted of an all-terrain vehicle (ATV) towing the transmitter and receiver coils. To make it robust on even harsh farm fields, the coils were mounted on sledges with runners. Moreover, a stationary version of the instrument had already been used in a cold environment during field campaigns in Antarctica.

The tTEM system was integrated in the Aarhus workbench software package for data processing, inversion and reporting.

HGG was contacted and questioned about the ability of tTEM to detect a titanium fan hub part buried under snow and ice. Their first feeling was that, due to the size and the nature of the part, its detection would be unlikely. Despite this, the scientists took advantage of the presence of a test fan hub fragment in Copenhagen, at the GEUS facilities to perform a detection test: the part, laying on the surface, was barely seen, its signal being at the noise level. The ability of the system to detect the real part under snow went, however, from unlikely to very likely, with some developments and adaptation.

2.3.1 tTEM description and ways of improvement

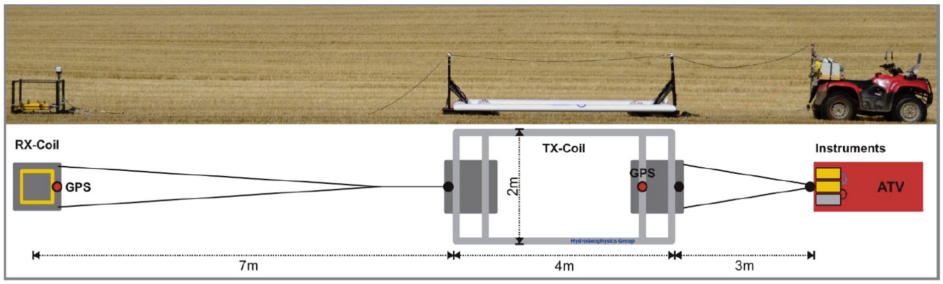

Source: HGG

Fig. 28: Picture of tTEM system and schematical overview of layout

The basic functionality of the tTEM system relies on a transmitter being abruptly shut off, which will introduce Eddy currents in the ground (Fig. 28). These Eddy currents will create a secondary magnetic field, and the decay of this field is measured with a receiver coil at the surface. The characteristics of this secondary field hold information on the subsurface electrical characteristics.

A detection test with the actual system “as-is” was carried out at a site in Funder, close to Silkeborg, Denmark, with relatively high resistivities, in order to get conditions that mimic those on ice and snow as closely as possible.

Source: HGG

Fig. 29: Picture of test setup: test hub placed 2 m from center of transmitter frame

The equipment remained immobile while the test part was moved around to see the signal responses to the different positions (see Fig. 29). As the part could not be placed below the tTEM system, it was placed at the side which is a less sensitive direction than directly below. In a real field case, the equipment would be moving across and over the part.

The conclusion drawn from this test was that the test hub could be detected by a tTEM type system. Nevertheless, the system signal to noise ratio (SNR) needed to be improved by an estimated factor of 10 to ensure a detection range of 5 m.

At the test site, the earth signal was low, but still much higher than what was expected in Greenland as ice and snow have very low electrical conductivity. In other words, all the operations needed to remove the earth signal would be unnecessary in Greenland and the uncertainties introduced by this operation would be avoided.

As previously explained, the setup used in the test had the test hub at the side of the transmitter. In a real situation, with the searched part being below the transmitter and as the electromagnetic coupling is higher below than to the side of the transmitter for a given distance, the situation would be favorable.

The piece of hub used for the test was about half the presumed size of the actual missing parts in Greenland: the test piece was one fifth of a 93% scale part, whereas the parts to be looked for were two fifths of a full-scale part in one case and three fifths in the other – see paragraph 1.1 From electromagnetic scaling laws, it was estimated that the signal from the actual missing part would be about twice the one of the test part.

The only way to improve the SNR was to improve the detection system, as the depth at which the missing part was located and its characteristics could not be worked on. The following developments were identified:

- Increasing the transmitter moment, by adding more turns to the coil, which would also increase the turn-off time, but as the test part signal was detectable outside the very early times, this was acceptable. The moment could be increased by about a factor of 4.
- Further increasing the transmitter moment by increasing the area of the transmitter coil. A factor of two could be achieved.
- Lowering the receiver coil noise level, by adding more turns to the coil. This would decrease the bandwidth of the coil, but again, due to the target characteristics this was not crucial. This would reduce the noise by an estimated factor of 4-6.
- Adjusting the gating of the signal, to decrease the noise level for this particular target. An estimated factor of 1.5-2 could be achieved.

In total, the modifications could significantly enhance the SNR, but counteracting this was a smaller stack-size in the real conditions as the platform would be moving (towed) to cover the search area. With the above developments, an improved SNR of about a factor of 10 to 15 was expected, taking into account that the missing part should have a higher response than the test hub.

Fig. 30 shows the signal obtained during the tests performed in Funder with the "as-is" tTEM system with the test fan hub fragment as a test part. The light green line is the noise level at this site. The red, pink, blue and black dots and lines are the signals measured with the test part located at 0, 2, 3 and 5 m from the center of the transmitter coil respectively. The dark green line is the noise level that would be expected in Greenland, with the improvements detailed above (the natural noise sources in Greenland are expected to be similar or lower compared to Funder). The grey area is the part of the signal that would be lost because of the system being moved over the measured area.

With the improvements described above, the chances of detecting a hub fragment part 5 m below the surface were reasonable. Consequently, it was decided to launch the developments.

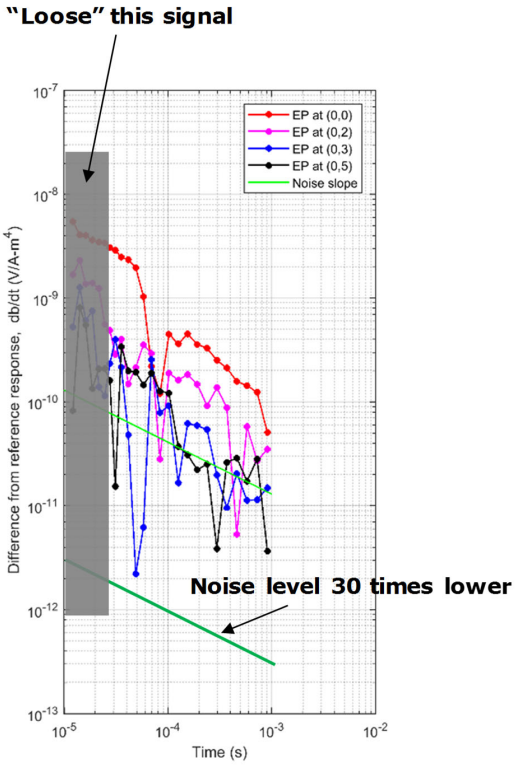

Source: HGG

Fig. 30: Signal measured during the tests in Funder

2.3.2 SnowTEM development and testing

The development of the SnowTEM version, as an updated version of the tTEM with the improvements described above, was launched early October 2018. A test in representative conditions was planned for early January 2019 as a go/no-go for a potential field campaign in the spring of 2019 with this sensor. The only period to go on the ice sheet being April/May and for logistical reasons, a decision had to be made three months before. This test consisted in burying the titanium test fan hub part under snow in a glacier environment, driving over it with the SnowTEM system and collecting data to estimate the maximum detection distance to the buried part.

Developing the SnowTEM, building it and testing it all within three months was a challenging task. Moreover, in case of success, it was decided to build two identical sensors for the field campaign, in order to have a backup. Both sensors could work at the same time for a maximum coverage. In case of a failure of one sensor, there would be spare parts and at least one unit still working.

The test location had to be as representative of the Greenlandic environment as possible. A test in Greenland was considered but the cost would have been prohibitive. Irrespective of the cost, timing required a mid-winter test, which added considerable levels of complication to the Greenland test.

The requirements were to be able to bury the test part under snow and/or ice, but also to have no bedrock or ground other than snow or ice over 20 m in depth. A glacier was the perfect location to carry out the test.

The temperature also had to be similar to conditions during the Greenland detection campaign, even if HGG had already successfully operated similar instruments during field campaigns in Antarctica. The behavior of the hardware had to be checked at low temperatures although it was not a major concern.

To have low temperatures and a glacier to work on, it was decided to go to Zermatt, in Switzerland. First, a glacier between the "Klein Matterhorn" and the "Breithorn" was identified, also called the "Breithorn Plateau" (Fig. 31). The main advantage was that it was accessible by gondola and ski lift, even if its altitude was higher than 3,800 m (it is indeed the highest point reachable by gondola in Europe).

Fig. 31: Initial test location, "Breithorn Plateau" in center, with Breithorn (4,164 m), on left hand side. View from Klein Matterhorn. "Gobba di Rollin" ski lift is just visible on right hand side. Crevasses downstream of the plateau are clearly visible

2.3.2.1 Test in Zermatt

The test was carried out from 14 to 20 January 2019.

It was led by GEUS, who coordinated with the Zermatt authorities, local search and rescue services and ski patrollers to arrange for the transportation of the sensor, team access to the test site, guidance and safety. This coordination was essential in order to ensure that the test was carried out in an appropriate location and within the limited timeframe.

The major difference between what was planned and what was actually performed was the location of the test site: due to strong winds expected during the week of the test, it was deemed unsafe by local safety guides to work on the Breithorn Plateau. A backup test site was proposed by the local authorities, also a glacier but at a lower altitude and more protected against the wind. This glacier was at the bottom of the "Theodulhorn", between two ski slopes (see Fig. 32). The thickness of the ice was estimated to be well in excess of 20 m. Two ski lifts were present at a distance of approximately 200 m on each side. At that distance, they were not a concern to HGG with regards to the sensor as they would not create any undesired signal.

A snowcat was used to carry people on site, and dig and bury the part under the snow. Two meters of snow covered the glacier ice (on the Greenland ice sheet, two winter seasons would have probably buried the real part under three meters of snow or more, plus impact depth). It was chosen not to dig further, to lay the part on the ice and to cover it with 3 m of snow. It was deemed acceptable to test the maximum detection distance with the part 3 m deep and with the SnowTEM not over the part but at a distance from its vertical. This would be conservative as the sensitivity is lower when the sensor is side-on compared to just over the target, for a same sensor-to-target distance.

It was also advantageous to have the snowcat with cabin close to the search site to protect the team from the elements during parts of the day. Outside temperatures reached -19°C, with winds up to 40 kt.

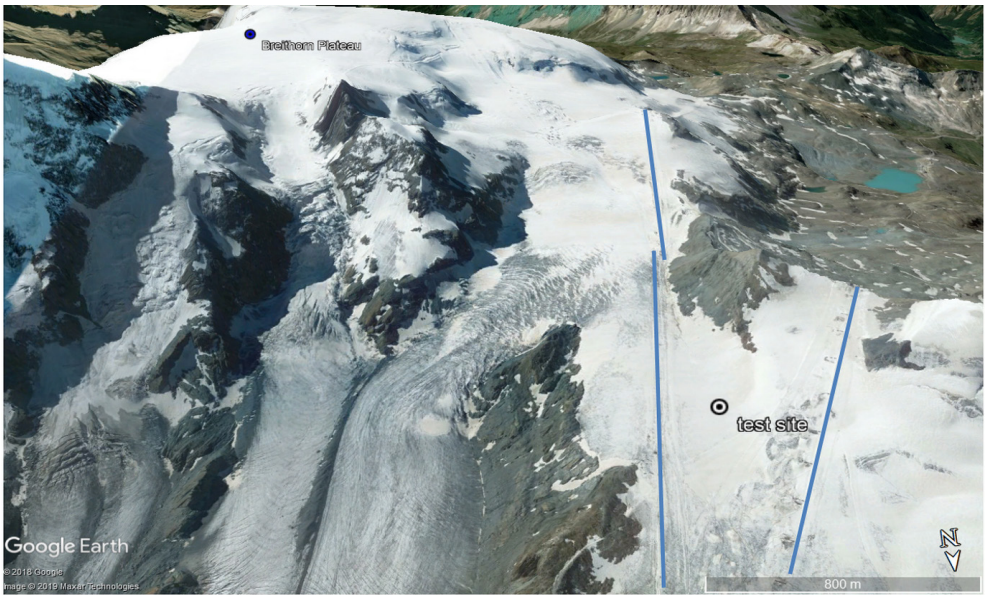

Fig. 32: Final location of the test site – closest ski lifts are shown with blue lines

2.3.2.2 Difficulties, results and steps forward

It rapidly became clear that this test would be unfruitful, as the noise level proved to be much higher on this test site than expected. It took time to affirm with certainty that the noise level seen during the test was due to the location of the site itself, and not the result of hardware malfunction.

The first on-site test did not detect the buried part. No signal was obtained above the noise level, even with the SnowTEM in a steady position just at the vertical of the part.

The cause of this noise was identified as being a power line that was, at its closest, 500 m from the test site as shown in Fig. 33. This line was not initially spotted as concerns had been focused on the ski lifts. To confirm this, measurements were done while moving towards and away from this power line. This confirmed that the closer to the line, the higher the noise. Results are shown in Fig. 34.

Spectral analysis of the noise showed that for the same time gates, the background noise level was 35 to 40 dB higher in Zermatt than in Funder. A test in Funder in Denmark was reproduced after Zermatt, and the results obtained before Zermatt (see paragraph 2.3.1) were confirmed.

However, the test in Zermatt made it possible to validate the mechanical behavior of the sensor towed by a snowmobile on a terrain which was, in certain points, similar to the search area in Greenland. In particular, the system behaved well when passing over sastrugi[19], with travel speeds up to 20 km/h (Fig. 35). The force needed to tow the sensor was also measured. Peak levels of 150 kg were reached.

Fig. 33: Location of power lines (red lines) and noise measurements (green dot)

[19] Sharp irregular grooves or ridges formed on a snow surface by wind erosion, saltation of snow particles, and deposition.

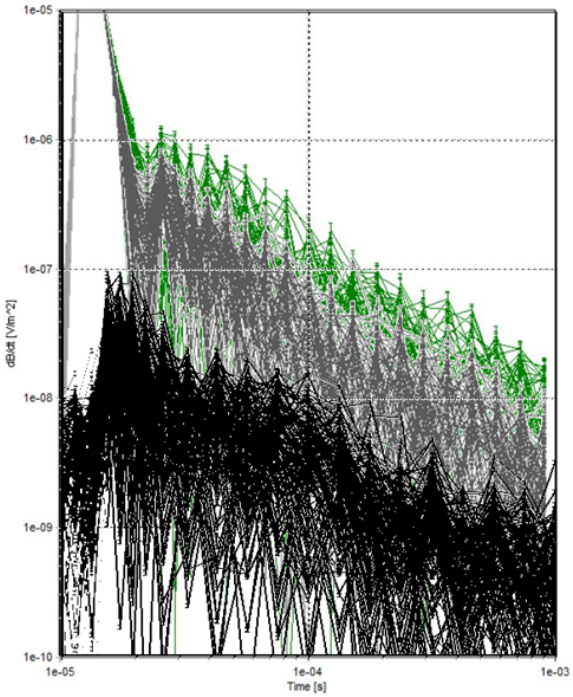

Fig. 34: Signal measurement with SnowTEM - close to the powerline in Zermatt (green), far from the powerline in Zermatt (grey), and measurement in Funder (black)

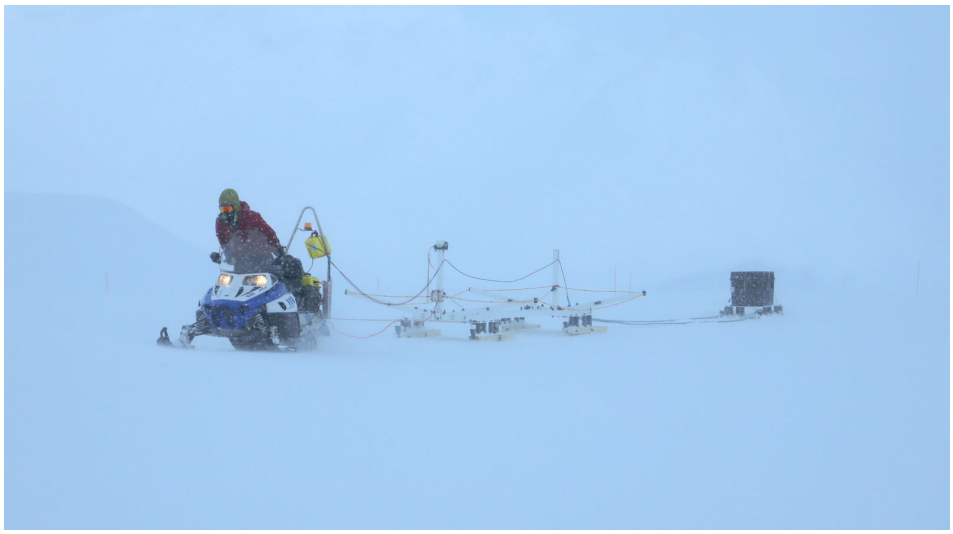

Fig. 35: Snowmobile towing SnowTEM during the test in Zermatt in low visibility conditions in a snow storm

2.3.2.3 Test in Sweden

The results of the test in Zermatt were not conclusive and did not add to the initial test done in Funder (Denmark). Therefore it was decided to carry out a last-minute second test of the SnowTEM, under snow. A site in Sweden was chosen, which turned out to be inaccessible. The search for an alternative spot was the only other possibility given the tight time frame of the test. This alternative spot had a significant geological response, yielding background noise. Even if the noise was low (about the level of Funder), the signal from the engine part was drowned in the signal from the ground.

The outcome of the test, once again, was inconclusive.

2.3.2.4 Numerical modeling and proposed improvements

Back in Denmark with still some uncertainties, HGG carried out numerical modelling in order to assess more precisely the measured response expected from the fan hub fragments, which were estimated to be twice the size of the test hub used for the detection tests.

The modelling showed that a part twice the size of the test hub would result in an increase in the signal strength by a factor of two. This added approximatively one meter to the detection range.

The influence of the distance between the transmitter and the receiver was also investigated. Based on a numerical analysis, the signal level would be increased by a factor of two if the distance was reduced from 6.8 m to 4.5 m. Gains were therefore achievable by slight modifications of the system.

A handful of driving tests were carried out in Funder, Denmark, with the configuration tested in Zermatt. The sensor was driven back and forth with an increasing distance to the test part. In this configuration, the part could be seen at a distance of up to 5 m from the center of the receiver frame when passing it. From this experience, a last improvement was proposed, consisting in adding an extra receiver coil in addition to the existing one. The detection range would be increased and the line spacing could be extended by 1 to 2 m.

2.3.3 Conclusion on the EM sensor evaluation

The SnowTEM sensor developed by HGG was tested in several places between October 2018 and February 2019. The aim of the first tests in Funder (Denmark) was to determine if a titanium part could be detected by the system and at what distance. This led to improvements of the system in order to increase the signal to noise ratio. In Zermatt (Switzerland), the objectives were to test the detection of a titanium part buried under snow on a glacier with the improved system. The sensor was towed with a snowmobile to also assess its mechanical behavior in conditions that were similar to what might be encountered during the survey in Greenland. The detection test in Zermatt was unfruitful due to unexpected noise levels, but the mechanical behavior of the system was satisfactory. A last test was rapidly set up in Sweden to assess detection under snow, which did not provide any new information due to the presence of a high earth signal. However, the tests made it possible to draw useful conclusions:

- The test hub could be detected at a distance of 5 m from the center of the coil. It was estimated that the mass of the missing hub parts was approximatively twice that of the test hub. Simulations showed that a gain of 1 m in the detection distance could be expected from these size and mass differences.
- The sleds built to carry the transmitter and the receiver behaved well on snow sastrugi. The force needed to tow the sleds was measured during the Zermatt tests with a force sensor. A maximum force of 150 kg was measured, which could be reduced, if necessary, by reducing the friction of the main sled. The use of a robot was envisaged, to tow the sensor during the intended field campaign. This robot had a theoretical towing capability of 100 kg, but no test could be carried out with the robot towing the SnowTEM due to availability, logistical and planning constraints.

- The low SNR encountered in Zermatt was due to power lines close to the test site. In the absence of power lines (as in Greenland), the SNR would allow the part to be seen at a distance of 5 m (6 m expected with real part). This was confirmed by the tests in Funder, even if the background signal of Funder was higher than expected in Greenland.
- No test with the part buried under snow and ice was conclusive. However, snow and ice behave as "free space" and their resistivity is at least the same or higher than the soil in Funder.

2.4 Conclusion regarding detection means and field campaign strategy

At the end of February 2019, the one and only evaluated system which was deemed able to operate in the search area environment and to detect the titanium fan hub fragments under the snow during a systematic search, and with reasonable confidence was the SnowTEM system. After the tests in Funder, in Zermatt and in Sweden and after the numerical modeling, HGG proposed a last set of modifications to the system. Compared to the setup used in Zermatt, the transmitter frame area would be increased from 4 x 3 m to 4 x 4 m. The number of coil turns of the transmitter would be increased from 3 to 4, and the power supply would be increased. An extra receiver coil would also be added. With these changes the SNR would be increased by a factor of 1.8 and the line spacing extended by 1 to 2 m. The distance between the transmitter and the receiver would be shortened, to increase the target signal response by a supplementary factor of 2.

For all these reasons, it was deemed acceptable to launch a new search campaign in Greenland in the spring of 2019. There were good chances that the SnowTEM would detect the missing part up to a distance of 5 to 6 m; the estimation was that the part was buried under 4 meters of snow after the winter season of 2018-2019. The manufacturing of two SnowTEM was launched in order to have a backup.

The Polar Research Equipment group[20] based in Hanover, New Hampshire, USA, was contacted. They developed and operate a 4-wheel autonomous vehicle, called "Frostyboy". It was known that this robot could carry a GPR or tow a sensor such as the SnowTEM in a harsh environment as it had already operated in Antarctica and in Greenland. The objective was to use it as a programmable autonomous vehicle to carry out search patterns for as long as its batteries permit, and to assess the safety level in crevasse fields for later surveys if safety was a concern for the snowmobile operators.

[20] https://www.polarresearchequipment.com/

A strategy for this spring field campaign was agreed, taking into account the new promising targets provided by ONERA and the available detection means. As for Camp Recovery in 2018, the field campaign was based on a live-in camp built in the search area, with 7 people present during a total duration of 4 weeks including 20 % of extra days due to weather holds-ups. The planned steps for this campaign were the following:

- perform a detection test with the SnowTEM sensor over the test hub buried on the ice sheet in 2018, to confirm its detection capabilities under snow,
- if the test is successful:
  - o survey the three high confidence ONERA targets with SnowTEM
  - o if no result from the ONERA targets is obtained, carry out a systematic search with the two SnowTEM sensors: one would be towed by the robot, the other by a snowmobile.
- If the test is unsuccessful, the campaign converts into a target check campaign:
  - survey the three high-confidence ONERA targets with GPR, as the GPR was still considered appropriate for a pinpoint search.

The field campaign was scheduled from 25 April to 20 May 2019. Field reports were daily sent to the investigation team, and daily decision making was delegated to the field team.

3 - PHASE III FIELD CAMPAIGN – CAMP RECOVERY 2

3.1 Logistics and planning

The departure base for Camp Recovery 2 (CR2) was Narsarsuaq, south Greenland, as for the Phase II field campaign (CR1), see (BEA, 2019).

The team was composed of three members from GEUS, two members from HGG (Aarhus University, Denmark) who developed the SnowTEM sensor and two members from PRE who were the Frostyboy robot operators.

A container was shipped from Copenhagen, holding the two SnowTEM detectors, the Frostyboy robot and all the equipment that could not be sourced in Greenland. Once in Narsarsuaq, on 21 April, 6,400 kg of equipment (including the container contents) had to be slung by helicopter onto the ice sheet. This represented nine sling flights.

On 25 April 2019, the first team members arrived at Narsarsuaq to start building the equipment slings. The objective was to have everyone on the ice sheet on 2 May.

Recent updates from the QAS_U weather station[21] suggested that there had been more snow accumulation during the past winter than the winter before. The weather station was buried, as happens in winter with high snow accumulation. Pleiades satellite images of the site of CR1, where flags had been used to locate the buried test hub during the Phase II search, were provided by Airbus with the acquisition dated April 2019. The flags were no longer visible. This meant that more than 1.5 m of snow was covering the area. GEUS took a second test hub fragment with them for calibration in case they could not locate the one which had been left on site marked by flags.

[21] See http://www.promice.org/ for further information about Greenland automatic weather stations.

The first four of the nine slings were moved to camp in good weather on 28 April.

The following days were non-flyable, with adverse weather conditions (from 29 April to 4 May). During these days, the team made progress by programming GPS units and tablets, and preparing for various potential scenarios. They practiced (on foot) navigating with the custom-built Google Earth setup designed to help cover the search area with 4 m line-spacing, they fine-tuned the snowmobile driving plans, discussed where and in which order the robot should map the crevasse field and also pitched tents inside the helicopter hanger so that they would be as familiar as possible with them while setting up camp on the ice.

On 5 May, it was still not possible to make a charter helicopter flight due to the weather conditions. The team started repacking the sling nets that had been sitting next to the runway for several days: items that were not needed due to the shorter campaign time were pulled. It was not possible to pull an entire sling load because the team had to anticipate a similar delay getting off the ice as they experienced getting on the ice.

On 10 May, the situation was still the same: no flight had been possible since 29 April due to weather, the team reconfigured the cargo and plans once again so as to get some people working on the ice sheet with a subset of equipment.

On 11 May, three sling nets with equipment were finally flown onto the ice sheet, along with five people. The equipment included a snow mobile (one was already on site since the first sling day), one GPR, one SnowTEM sensor and the robot. A Stronghold dome tent and toilet tent were set up rapidly as another storm was advancing into the region. The first work consisted of digging out slings that had spent the previous ten days on site. The predicted storm indeed hit the camp on 12 May, preventing any survey, and any generator functioning – thus crucial battery charging. The day after, good weather allowed some work which consisted of assembling a large Polar Haven tent, moving the gear into it, then digging the camp out of accumulated snow drift. The snow mobile was encased in snow and refrozen ice and it took several hours of work to free it. Another storm hit the camp after one hour of GPR calibration and line driving to test the sensor, with strong winds and blowing snow. The next day (14 May) was unworkable due to bad weather.

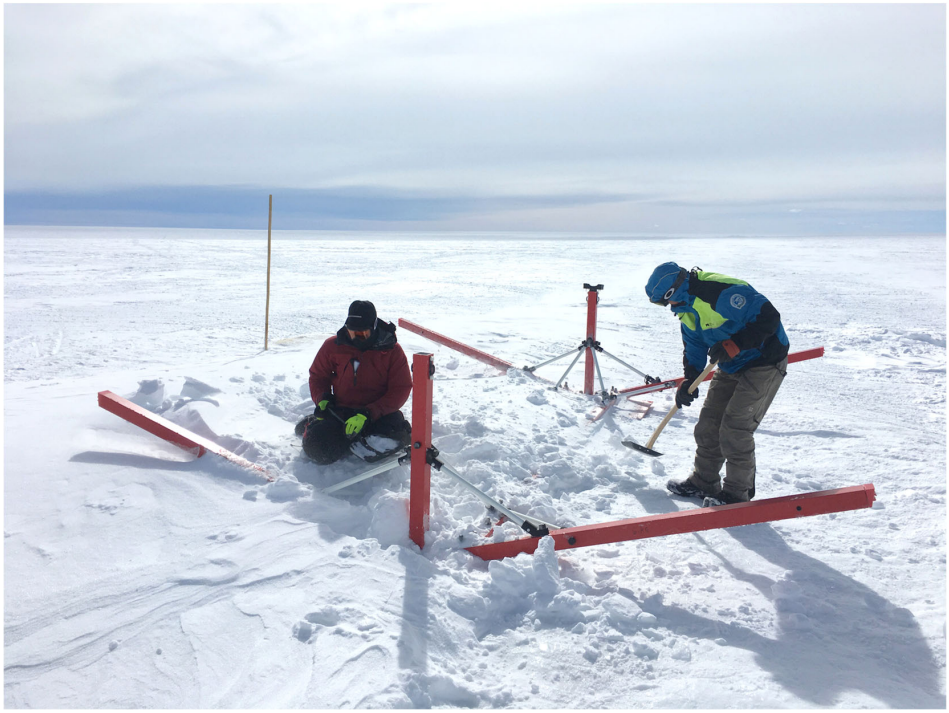

Fig. 36: Digging out one of the two SnowTEM systems after a snowstorm

On 15 May, one last person joined the camp with a last helicopter sling. Assembly and testing of the SnowTEM sensor started and lasted until the next day. Calibration work began over the buried test hub location from the previous year. Unfortunately, without the flags and because of the ice sheet drift, its exact location was not known.

A few days before, the team decided to take advantage of the helicopter flights in to improvise a drop test from the helicopter with the second test hub fragment, to better estimate the impact depth of the part being looked for. The part was dropped by the pilot at around 1,000 ft above the ground. It was unfortunately dropped more than one kilometer from the camp and almost over the horizon resulting in this part being lost.

3.2 Ground search campaign

On 17 May, there were new issues: first, the 2 kW generators required to charge the robot batteries only put out 1.5 kW, which was not sufficient. A new generator (stating "4,500" on the side but actually furnishing 2.6 kW) was airlifted the day after. This solved the problem.

Second, the high accuracy GPSs which were specifically rented because they had a high precision feature providing position accuracy to 10 cm could not be enabled. This option was needed to accurately estimate ice velocity. This was solved on 20 May after many calls to the supplier and insistence from the AIB DK, it appeared to be a configuration issue.

Despite these problems, a point of interest where the test hub of the previous year was supposed to be was just about detected with the SnowTEM sensor. Multiple passes over the point of interest confirmed the presence of the test hub. However, it also highlighted that the noise introduced by driving swamped the SnowTEM signal, so the part was only visible when the system was stationary.

At this stage, the planned systematic search campaign turned into a pinpoint search campaign, because of both the sensor motion noise, and the extensive weather delays accumulated so far.

The displacement of the detected test part versus the coordinates at which it was buried was estimated at 62 m, south-southwest. This was used to reduce the survey area for the three ONERA targets.

Fig. 37: Base camp for ground search campaign – Photo: Rune Ellerup Kraghede

For each of the three ONERA targets (1, 2a, 2b, Fig. 20), the process was to search the area from the ONERA target position, using improved ice velocity estimates and then move outward, stopping every meter. Instead of marking objects with a high-precision GPS unit, the use of analog methods was preferred - bamboo stakes, flags, and even juice concentrate, to mark the snow. The FrostyBoy robot did autonomous safety assessments of crevasses in the ONERA 1 and 2b target regions, while the SnowTEM surveyed 2a. Later on, FrostyBoy and its GPR saw crevasses within 5 m of the surface near ONERA target 1.

In addition, the team realized that the last SnowTEM design modifications decided after the Zermatt test, which consisted in enlarging the transmitter frame and doubling the number of receiver coils, made the assembly heavier, meaning that the robot was no longer able to pull it. It could now only be moved manually or with a snowmobile.

Based on this, it was decided to walk in on ropes rather than drive in on the snowmobile to reach ONERA Target 1. Consequently, the SnowTEM sensor was rebuilt removing the skis, platforms and arms, so that it was quite similar to the HGG WalkTEM: a 4 m x 4 m cable held in a square shape by bamboo poles that can be dragged on the ground. It was tested over the buried test part. The new sensor setup could be pulled to target 1 on a sled behind a roped team, or easily flown in by helicopter for a day of work that would avoid the crevasses between the camp and the target, leaving the team to deal only with those directly under the search area.

The FrostyBoy safety assessment of target 2b was acceptable: 90% of the search area was between crevasses and not over them.

On 20 May, the SnowTEM team completed the analysis of target 2a. Results were negative: their conclusion was that "it is highly unlikely that anything equal-or-larger and equal-or-shallower than the test part was within the search area".

Thanks to the FrostyBoy crevasse mapping over 2b, a (relatively) safe path to the search zone of target 2b was selected. The edges of the two crevasses which had to be crossed were marked. The first crevasse was safe with a width of 2.5 m and a snow bridge thickness of 10 m. The second was fairly safe with a width of 6 m and a snow bridge thickness of 6 m. Unfortunately, the 2b search area was found to be partially over a crevasse of a width of 4.5 m and with a bridge of 2 m which could be crossed on foot but not with a snowmobile.

On 21 May, to gain confidence in the capabilities of the SnowTEM sensor, it was decided to dig out the test hub. It took 9.5 hours to dig a 4.2 m deep by 2.2 m wide hole, and a hypotenuse ramp 9.2 m long, and to remove nearly 40 m^3 of snow (i.e. 20 tons). The team used a chainsaw, two hand-saws, a drill with a 2 m corer, two snowmobiles, two large tub-sleds towed behind the snowmobiles, and about 10 shovels to move chunks of ice weighing 40 kg among all the snow.

The test part buried the year before was spotted exactly where the SnowTEM had detected it. An hour later it was still stuck in ice at the bottom of the hole and work was stopped for the night. Overnight an unexpected storm came in and filled in the hole. So a second 4.2 m deep hole in the same place as 24 hours earlier had to be dug. This time it took three people and two hours to reach the part rather than five people and ten hours: the total volume of snow was similar, but the weight was probably one third of the previous snow because it was freshly drifted and had not been compacted for two years. After touching the test part, it took about 15 minutes more to free it.

Target 2b was also surveyed, in an area where the team thought the target would have moved to based on further ice flow analysis. No response was obtained.

The FrostyBoy survey of target 1 established that there were eleven crevasses between the camp and target 1, but all had snow bridges greater than the crevasse width. The team decided that it was safer to use a helicopter to go to target 1. The plan was to use the SnowTEM and search an approximately 10 by 25 m area in which the ONERA target was believed to have landed. If anything was detected, it would be marked and further actions figured out. Indeed, digging had been very difficult with all the equipment mentioned above, and at this crevasse-rich site it would probably have to be done just by hand to ensure workers' safety.

On 23 May, the team cleared 2b with null result.

3.3 Positive signal response

On 23 May, it was fairly windy but the helicopter pilot arrived in camp and flew four people out to target 1. Despite the wind blowing which made the work difficult, the team managed to assemble the lightweight SnowTEM and within five minutes of operation had a clear and unambiguous signal that a large piece of metal was nearby. It was located in the southwest corner of the search box defined around the target from ice velocity assessments. This unambiguous signal was consistent with an anomalous signal detected by FrostyBoy and its GPR during the crevasse surveys several days earlier. The depth of the top of the object was estimated at three to four meters. Some time was spent fighting the wind and localizing the maximum strength of the signal, then the team marked the spot with flags and juice, marked the two nearby crevasses with flags (see Fig. 38), and returned to the camp.

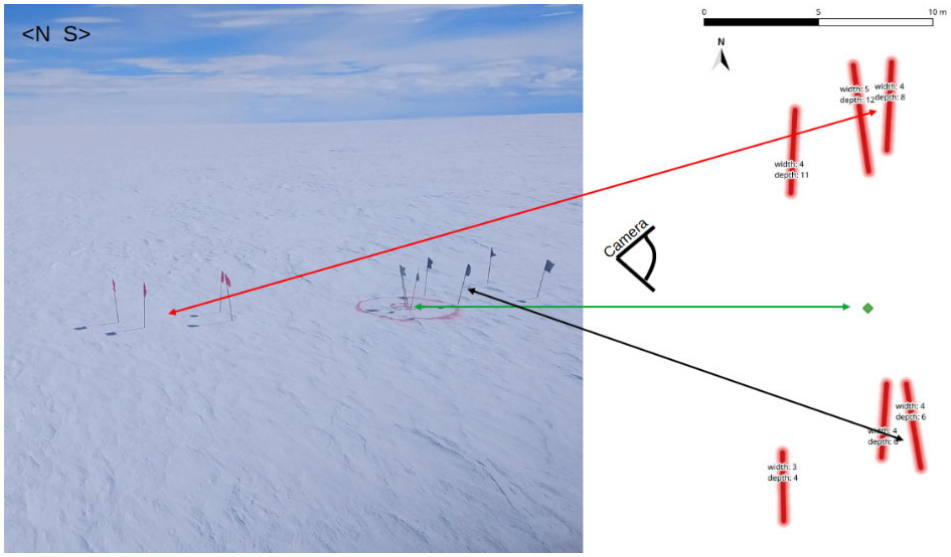

Source: Thue Bording (HGG)

Fig. 38: Location of target 1 signal (red circle), and nearby crevasses (four orange flags on left hand side and four black flags on right hand side). Photo is taken from west looking east. Crevasses run east/west. Crevasse locations outside of orange and black markers are uncertain. Distance from target center to edge of black-flagged crevasse is 2 m. Distance from target center to edge of orange-flagged crevasse is 5 m. Black-flagged crevasse width is 4 m, bridge thickness 6 m. Orange-flagged crevasse width is 4 m, thickness 8 m. Also barely visible in image running left/right near bottom are FrostyBoy tracks.

As it took six people and ten hours to dig out the test part with significant mechanical support, no nearby crevasses, and no ropes, the team expected it to take much longer to dig out the real part.

In accordance with the general schedule of the Phase III search, two people including the glacier safety guide had to leave the camp that day. Yet another storm was forecast for the day after, prohibiting any helicopter flight and any outdoor work.

The initial planning was to start pulling out of camp on 22 May. The majority of the team members had flights home on 28 May at the latest, with no possibility of postponing them due to other commitments. The detection occurred on 23 May, and on 24 and 25 May a storm did indeed hit camp. The few remaining expedition days were not enough to excavate the part with the gear available while not damaging it. Furthermore, the unfortunate proximity of the crevasses was clearly a safety issue and required specific safety gear. In such conditions, the time to excavate the part was estimated to be 20 to 40 hours of digging with five people.

It was then decided with the investigation team that the excavation phase would be a further, separate and dedicated campaign.

On 26 May, the team performed a dense GPR survey that was critical for the safety of a potential future dig team. They also built some slings for pull out of the camp.

27 May was the last day on ice for the team members. They finished the dense GPR survey of the detection area around target 1, concluding that the snow bridges immediately around the detection were a bit thicker than the previous estimate. They also used the lightweight SnowTEM a last time to try to refine the detection location to within one meter.

The precise detection location was:

61.735026 N
46.853879 W

This position was 71 m south-southwest from the location of target 1 provided by ONERA as a result of ice movement since the SAR data acquisition of Phase II.

All members returned to Narsarsuaq on 27 May, leaving six slings on the ice which would be recovered later, depending on the extraction campaign needs. This marked the end of camp recovery 2.

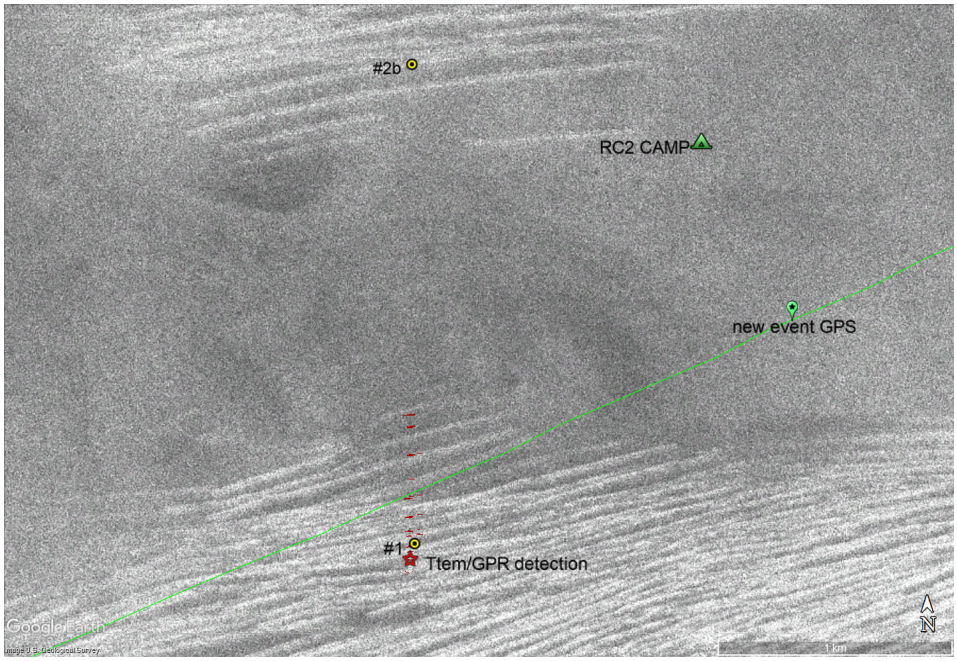

Fig. 39: Location of detection (red star) – yellow circles are ONERA target locations, white stripes are crevasses as seen on UHF images, red markings are crevasse edge detections

4 - EXTRACTION

The extraction phase following CR2 was discussed just after the team left the ice sheet and an extraction campaign was set up for end of June 2019. It was necessary to go back to the ice as soon as possible, so as not to be confronted with the disappearance of any markings and with ice flow that would have required a new search for the part.

4.1 Overview

Based on the effort to dig out the test part and the location of the target, GEUS estimated that the extraction would take a team of five people working 20 to 40 hours.

The AS350 helicopter used for CR2 could not move five passengers both to and from the target on one tank of fuel, nor could it move any extra equipment with five passengers, so four extra flights would be required to bring in the equipment.

Given these requirements, two days were scheduled to sling in, then four days of digging (32 hours on a basis of eight hours/day), and two days to sling out. Four weather-delay buffer days were included, plus two Sundays (pilot rest days) which could be swapped with nearby days. This meant twelve working days out of 14 possible days. As with CR2, in a worst-case scenario, the return slings could always be delayed.

The plan was to remove the first meter of snow and ice by cutting snow blocks with hand- and chain- saws, and then to shovel the blocks out of the pit. The second and half of the third meter would be removed in the same way, but a ramp would be added, snow would be shoveled into a sled, and the sled would be pulled out of the pit using either a mechanical winch/pulley, or man-hauled via pulley if necessary. At this point, work would slow down so that the diggers would not damage the part as they approached it. The final 0.5 to 1 m would be melted by heater so as to avoid touching the part with shovels or saws.

Even if the mission was planned to be Narsarsuaq-based, last not more than a few days, and was only dedicated to the extraction of a part which was already located, supplies to be slung in included a large amount of gear: three barrels of jet fuel to refuel the helicopter in the field, a winch, a heater to melt the snow and ice, two barrels of benzine to operate the winch and the heater, tent and plywood to cover the hole so that it did not fill in overnight, supplies such as shovels, chain saws, etc., and safety equipment (rope, carabiners, food, fall-arrest system, etc.).

Some of this equipment was already on the ice from CR2, so part of the first day would be spent digging these slings free from snowdrift buildup, and then moving equipment from CR2 to the target location, rather than slinging it in from Narsarsuaq.

4.2 Development of campaign

A member of the Polar Research Equipment (PRE) team left Boston on 21 June to fly to Narsarsuaq via Reykjavik. A project leader from Greenland Guidance and a member from the GEUS team joined him on 22 June.

The first days in Narsarsuaq were dedicated to collecting the various pieces of equipment that had been shipped for the campaign: a hoist, a Herman Nelson heater, an electric chainsaw (backup for the gas-powered one that had remained on the ice from the previous month), some extra harnesses.

On 25 June, three members from the Iceland Search and Rescue (ISAR) team joined the group. The first helicopter flights were planned for 24 June, but weather did not permit any flight before the 28th (see Fig. 40). This meant that the initial hold-up due to weather was already four days.

During this period, the team developed scenarios involving minimum need-to-have versus nice-to-have equipment, and had preliminary discussions about not excavating the fan hub in several day-trips from Narsarsuaq, but rebuilding an on-ice camp and staying up there to reduce their reliance on helicopters. Indeed, the initial plan was to fly the team members in and out by helicopter every day.

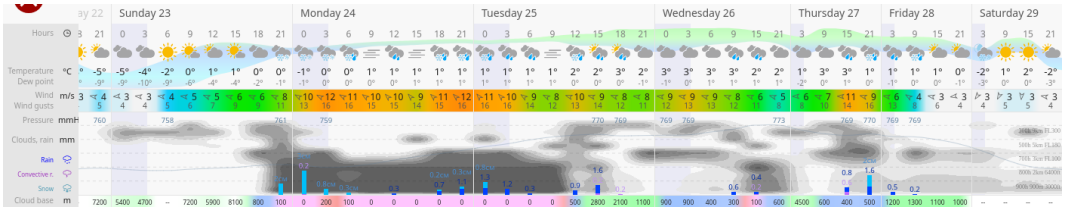

Fig. 40: Weather forecast from 22 June on search site, windy.com

Risks were also evaluated regarding the possibility of a hole collapse. Indeed, large volumes of meltwater, due to either recent rain events or the planned use of a heater to melt ice, may weaken the snow structure surrounding the crevasse. The probability was evaluated to be between “unlikely” and “possible”, while the severity was estimated as “moderate” as the team was prepared and planned to be secured by a multi-anchored fall arrest system.

A carpenter in Narsarsuaq built a winch platform, and sawed a fuel barrel in half to get a U-shape lip-protector for the hole to be dug so that the winch cable would not cut into the snow.

Given new weather hold-ups (see Fig. 41), the new plan was to fly three passengers to the disassembled CR2 site, move the five slings which were still there to the target, move the passengers to the target, and check that the stove, rifles, and one tent had survived the month on-ice, at which point the helicopter could leave, and work could begin.

In the camp-on-ice scenario, “work“ would involve not just digging but spending a lot of time in survival mode: cooking and maintaining camp. It was hoped that a second flight with more passengers and the heater, and then a final flight with the last passenger would arrive soon after, not days after, to help maintain camp and dig and melt the hole.

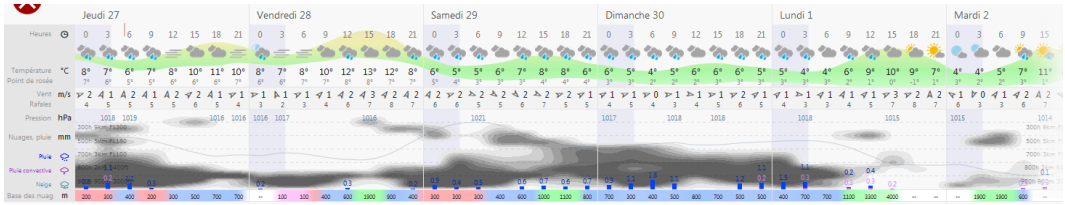

Fig. 41: Weather forecast from 27 June on search site, windy.com

On 28 June, a first helicopter took off with three team members, their survival gear, safety gear and some supplies - a winch, drill and generator. They were dropped off among the six slings and fuel drums that made up the disassembled CR2 site. After finding the rifle to protect the team against polar bears, a tent bag, and making sure that the stove could be turned on, the helicopter left them there to dig the slings out and break them free from the ice. The helicopter returned to Narsarsuaq and picked up two other members, flew them to CR2, moved four slings from CR2 to the excavation zone, moved all five passengers to it, and then returned again to Narsarsuaq with one snowmobile sling.

A third flight delivered one sling with the Herman Nelson heater and an extra drum of fuel, and returned with the second snowmobile. The camp was set up. An aerial picture of the camp during the excavation phase is shown in Fig. 42.

The manual digging started that same day. At 11:00, a depth of 1.1 m was reached. Weather was getting worse. Snow was falling and winds were gusting to 8 m/s, but work continued. At 14:00, the team was at a depth of 2 m. Digging without the winch stopped; the use of the winch to haul sleds of snow out of the pit started, which made life much easier for the workers.

At 17:45, a shovel came twice into contact with a metallic part. Both contacts were at approximately the same location. As per the protocol, the shovel/part contact point was marked on the part.

The team started to melt out the part with the Herman Nelson heater to avoid further metal to metal contact. Six fan blades, attached to what appeared to be a hub fragment, were found cut in half. The shovel contacts were with the fracture surface of a fan blade.

It was confirmed at that time that this part was a fragment of the hub with blades attached.

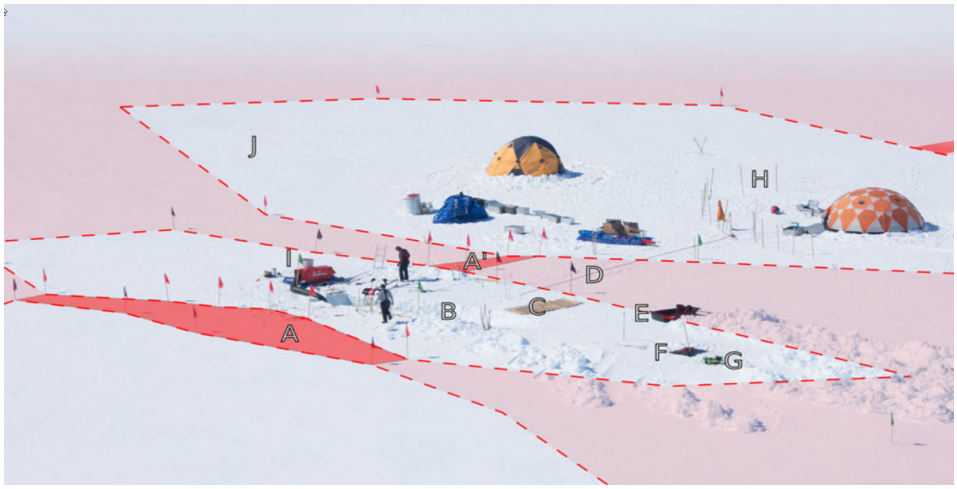

Fig. 42: Photograph from helicopter of excavation work-site as described in (Mankoff, et al., 2020). (A and A') Dark red graphic overlays between flags mark known crevasse locations as detected by GPR and DGNSS. Dashed lines enclose safe areas and pink marks unsafe areas defined with GPR data, the UHF basemap (Fig. 21), extensive snow probing and crevasse location uncertainty with distance from known crevasse locations. (B) Ramp out of pit. (C) Plywood used to cover pit overnight to prevent drifting snow filling. (D) Safety rope bridging crevasse between the northern (far) camp island and the southern (near) work island. (E) Sled. (F) Winch and winch platform. (G) Generator used to power winch. (H) Bamboo poles marking polar bear alarm trip-wire surrounding sleep tent. (I) Herman Nelson heater, hose and fuel barrel. (J) Helicopter landing zone. Photo by Austin Lines.

The part was unfortunately embedded in the side of the pit facing the crevasse, so the team had to melt toward the crevasse wall. They planned to attach ropes and anchor the part as soon as they could find an attachment point on the fan hub encased in the ice.

The top of the fan blade where contact was made was at an approximate depth of 300 cm and around 30 cm below the 2017 impact surface determined from the solid ice layers. This was in accordance with the hypothesis taken by ONERA for their radar image analysis, as described in paragraph 1.3.5.

Melting of the part paused between midnight (40% melted out) and 08:00 the next morning. Melting continued throughout the day (Fig. 43 and Fig. 44). Even after the part was melted free, it took significant effort to then get it out of the hole. There were no good attachment points and sharp metallic fractured edges cut the ropes wrapped around the part. Finally, a three degree-of-freedom hoist mechanism was built by hand and the part was lifted, placed onto a sled, and hauled to the surface.

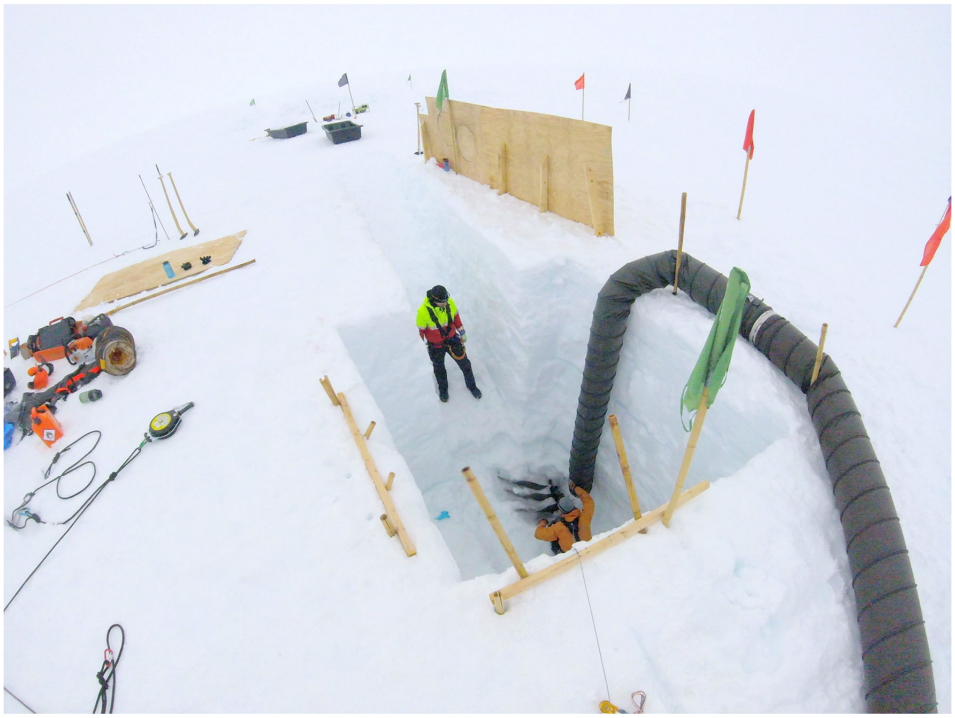

Fig. 43: Melting out snow and ice around part in 4 m deep hole. Photo by Arnar Ingi Gunnarsson

Fig. 44: Photo by Dirk van As, Greenland Guidance. Photo of Icelandic rescuer melting out fan hub

The part was slung to Narsarsuaq and arrived at 18:45. Despite previous cautions and warnings, additional metal/fan blade contact occurred after the part was on the ground when the helicopter, still hovering directly over it, released the net hooks. The metal net hooks fell straight down and dented a fan blade. The location of the dent was marked. This dent did not affect the investigation into the root cause of the fan hub failure.

A final helicopter flight retrieved the five members of the on-ice digging team. Prior to leaving the dig site they tore down most of camp, but work remained: slings still had to be moved from the crevasse field to a local safe zone where pilots could pick them up without assistance, and then move them all to town.

On 6 July, a safety investigator from the BEA, one from the NTSB, and another from EA met in the hangar in Narsarsuaq to take the first detailed pictures of the part and its fracture surfaces, before putting it in a sealed crate for transportation to P&W for further examination.

The aircraft which was chartered by EA to transport the part from Narsarsuaq to P&W, East Hartford, Connecticut could not take off from Narsarsuaq on 8 July as scheduled, because of strong winds.

It finally took off on 10 July. The day after, the examination of the fan hub and blades started at P&W, under BEA supervision.

Fig. 45: Loading of crate with fan hub into transport aircraft, an Antonov 12

5 - LESSONS LEARNED

5.1 Safety

A few days after the F-HPJE event, an Air Greenland helicopter was rerouted to locate and recover pieces of debris. Landsat data gathered shortly after the event (see Fig. 46) did not reveal any surface crevasse in the area. Neither did TerraSar X images of the area.

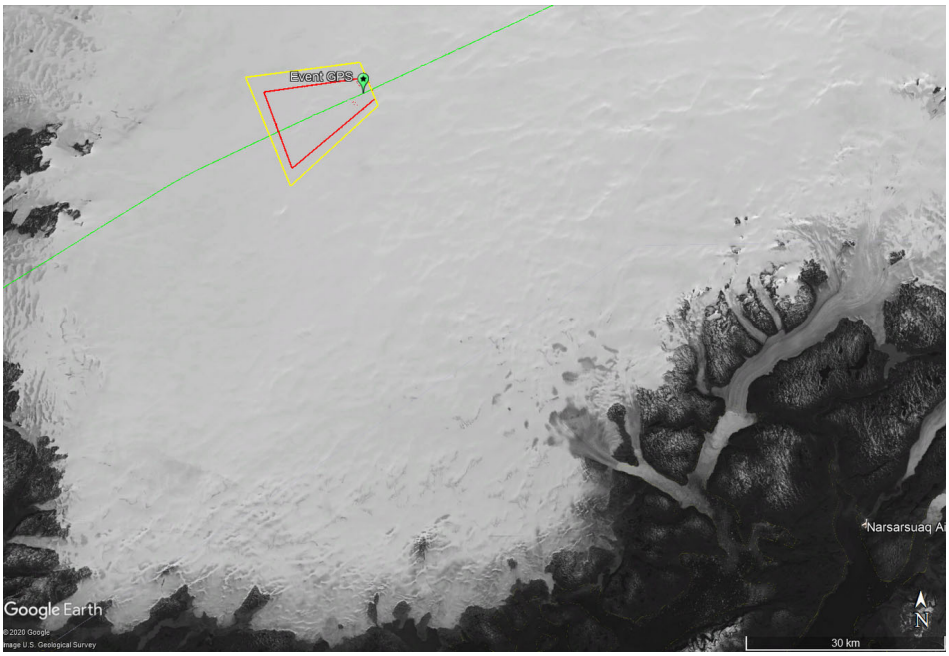

Fig. 46: Position of event and first areas of searches. Background is a Landsat 8 image of South Greenland. Yellow and red areas were provided to Air Greenland for helicopter survey

During the survey by Air Greenland, the helicopter landed several times on the ice sheet and the pilot left the helicopter and walked several tens of meters.

Once the SAR campaign had been performed, analyses of the acquired images showed that the search area was surrounded by snow-covered crevasse fields (Fig. 47). Luckily, the majority of the debris was located outside of these crevasse fields. According to (Mankoff, et al., 2020), given that ~50 % of the region […] is a crevasse zone, and crevasse density may be ~20 %, we estimate up to a ~10 % chance of landing on a crevasse or first-step out of a helicopter is over a crevasse, and an almost 100 % chance of crossing a crevasse if moving just a few tens of meters, with possible fatal consequences.

A thorough regional geophysical survey should be done before any operational field work in order to assess the risks and to collect the initial data needed to interpret later geophysical data products. If such data are not available, extreme caution should be taken when first landing in an area.

An alternative means for the global assessment of the potential presence of crevasses via satellite radar imagery in the L-band is the ALOS PALSAR, a Japanese instrument. It was not used during this campaign as it was discovered that there were crevasses when the airborne radar imagery was processed, which had a better resolution than the Japanese SAR. It would be interesting to assess if these crevasses are visible in a PALSAR image for future deployment. P-Band SAR was found to be the best option to detect crevasses and a future ESA mission will include a P-Band SAR in space, called BIOMASS. However, the resolution of BIOMASS is too coarse to be of interest for that purpose.

During the field campaigns, the SAR crevasse map was used to determine safe survey areas. The safety of areas with visible crevasses on the SAR map was assessed via a GPR survey before any systematic search, looking at bridge thickness versus crevasse width. Target surveys in these areas were performed by roped up people.

The presence of crevasses also forms a limitation in terms of schedule. The best period for organizing a field campaign is April-May. Before April, the days are short, the weather is too adverse, storms are too frequent, and there are very few chances of having good conditions for helicopter flights. After May, during warm events, the snow surface will start melting and percolating down so that snow bridges over crevasses become weaker.

Apart from crevasses, the other major risk in terms of safety is the potential presence of polar bears. As the camp was relatively small, one of the protections was an alarm trip-wire which surrounded the sleeping tents. All of the campers had also undergone survival training which included the use of rifles and pyrotechnic flares to scare away polar bears. The alarm trip-wire is good for small camps, but becomes inappropriate for big camps.

During the field campaigns, no polar bear was spotted on the different camps. However, one was spotted close to homes on the other side of the fjord when the team was blocked in Narsarsuaq in May 2019. Shortly after, it was seen swimming across the fjord towards Narsarsuaq, but was not sighted again.

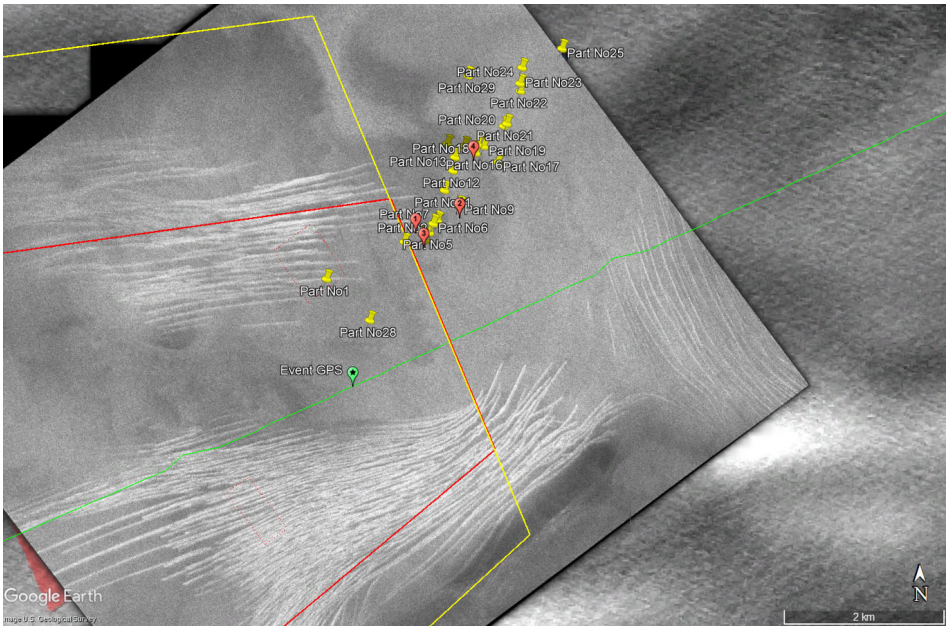

Fig. 47: Pieces of debris found by Air Greenland (yellow plots). Foreground map is UHF image of search area acquired during air campaign of April 2018. Crevasses are clearly visible in white. The background is TerraSar X image of area

5.2 Organization

In the scope of the BEA's safety investigation and for obvious flight safety reasons, the main objective was to try to recover the fan hub fragments as quickly as possible, as it was key to determining the root cause of the fan separation.

However, this technical and human experience showed that organization considerations have to be taken into account. This paragraph deals with organization recommendations so as to be as effective as possible for further search of this kind. Some parts of this paragraph are extracts from (Mankoff, et al., 2020).

Detection, localization, and extraction campaigns should be separate because not all the information may be available until previous steps have been completed.

A thorough regional geophysical survey should be done before aerial surveys and the operational field work to assess risks and to collect the initial data. For example, positioning DGNSS transmitters, corner reflectors, and collecting snow density measurements.

The SAR overflight was unable to initially detect the test fan hub fragment, requiring large search-area campaigns instead of a targeted search campaign. Extensive algorithm development time and processing was required to generate three potential targets.

Only one of at least two fan hub fragments was found, however no other salient target was detected in the wide area scanned by the SAR during the ONERA campaign. Not finding the other hub debris did not impact the root cause investigation.

Sensor validation and testing should be done with test parts as similar as possible to the parts which are being looked for. In this project, the test part was critical to sensor validation and algorithm development. It was one fifth of a 93% scale fan hub and was used for empirically testing the instrumentation. The actual part was an unknown portion of a full-scale fan hub. It ended up being just over 50 %, plus parts of nine attached fan blades. Using the significantly smaller test part complicated detection ability testing with both the SnowTEM and GPRs.

The SnowTEM detection capability in motion was also tested successfully in Funder, but with the test part lying on the ground, not buried under snow. On the field, the SnowTEM was only able to detect the smaller, buried test fragment when stationary, and based on this it was decided to perform go-stop-go measurements. A full wide-area search with this approach was neither practical, nor possible within the time-frame available. This was less critical as extensive weather delays at the beginning of CR2 had changed the focus from wide-area searching to pinpoint searches (see paragraph 3). The actual fan hub part would have probably been detectable with the SnowTEM in motion. Its actual signal may have resulted in fewer false-negatives with GPRs and, from knowing what signal to look for, fewer false positives where signal to noise ratio was too questionable.

If developing new instruments, adapting existing instruments for new targets, or training operators on new targets, analog field trials of sensing instrumentation before mounting a full-scale search-and-recovery effort are strongly recommended for future campaigns. **The best analog field site for trials of sensing instrumentation is on-site**, in or adjacent to the actual search area. This avoids widely varying snow and ice conditions between different regions of the ice sheet, or the ice sheet and an alpine environment.

Tests should be performed in conditions as close as those expected on site. For example, the tow capabilities of FrostyBoy did not match the towed load of the SnowTEM, and as such could not be used to tow the SnowTEM in the crevasse field. Due to logistical and availability reasons, it was not possible to test this configuration in Zermatt, but towing force measurements were performed, which proved insufficient. It is however possible to reduce the towed load of the SnowTEM for future applications, or use more powerful autonomous vehicles.

5.3 Means of detection

During the aerial survey in April 2018, multiple resolutions and multiple sensors were used. Multiple resolutions means low (e.g. Landsat 30 m/pixel) through high (cm) resolution satellite imagery, followed by low through high resolution airborne overflights. Multiple sensors should be used because until these types of surveys become common, it is uncertain which sensors respond best to the different debris shapes, sizes, materials, and surfaces. Surveys should be redundant (i.e. multiple passes with the same sensor) so that stacking and averaging algorithms can be applied. Different observation geometries of the research zone are recommended, in terms of heading and in terms of incidence angles (the SAR is a side looking instrument).

If the area and the debris are covered with snow, SAR data should be acquired as the electromagnetic waves can penetrate dry snow. Resolution is a key issue, as well as frequency. The resolution has to be better than the object to be observed. For example for crevasses, the resolution has to be better than 5 m, which is compatible with the ALOS mission performance. For the detection of an object around 1 m, a resolution of around 50 cm is needed, which is not available from space for commercial missions.

The choice of frequency is a key point. Lower frequencies penetrate deeper than higher frequencies. It could be concluded that the lower the frequency, the better. In fact this is a wrong perception. The image pixel containing the object will be composed of the combined response of the natural media over a depth of the order of the penetration capability and the response of the object attenuated by the depth of snow covering the object. The depth of the object is given. So to maximise the detectability of the object, one has to maximise the response of the object with respect to the background contribution which can also mean minimising the attenuation and the background response. At lower frequencies, the attenuation is minimised but the response of the media is maximised with deeper contribution. At higher frequencies, the attenuation through the medium is higher but the column of snow impacting the response is smaller.

Resolution is the major key factor and in general, higher resolution can be achieved with higher frequencies. It is thus recommended to use the frequency allowing a penetration which is compatible with the expected object depth.

During Phase I, satellite imagery was considered to look for visible fragments on the ice sheet surface. It appeared that there were not enough stationary visible patterns (such as rivers, coastlines, lakes) on the images to correctly reference the images to earth coordinates. Even if a part had been spotted, it would have been impossible to get its GPS coordinates with a precision below 200 m, as it was observed that the shift between real pattern positions on the ice sheet and their coordinates on satellite imagery could reach 200 m.

The first ground field campaign (CR1) led by GEUS, in May 2018 just after the aerial campaign, was based on the use of 250 MHz and 800 MHz MALÅ GPRs towed by snowmobiles. GPR had previously been used to map the extent and depth of metal and other debris within the Greenland ice sheet (Karlsson NB, 2019). However, the depth, sizes, and material were different: Karlsson observed a small military base of various materials buried 100 m deep, while here a titanium object of roughly 1 m^3 buried 1 to 2 m deep was being looked for.

Detection tests of the test hub buried under snow quickly showed that the GPR was not optimal for a survey of large areas. Indeed, the 800 MHz antenna did not detect it when driving over it. The 250 MHz antenna was able to detect it depending on which direction the snowmobile was driving (i.e. depending on the orientation of the piece relative to the radar). However, detection was not always successful. In addition, the signal from the test fan hub was similar to the signal from the various ice lenses throughout the snow in the search area: detections were identified in the GPR data near most of the ONERA targets, but after digging only ice lenses were found: the GPR false positives also occurred in the SAR data. Finally, when the test fan hub was detected it was only when directly over it, meaning that dense 1 m track spacing was required, greatly reducing the size of a possible search area to that initially expected given fixed time constraints.

GPR was used by roped team-members to probe the crevasse field periphery. It indicated crevasses with what appeared to be snow bridges less than 3 m thick and with down-warping layers. GEUS therefore did not search in the crevasse field, but determined that it was possible with other personnel and an autonomous vehicle.

The second field campaign (CR2) also led by GEUS, in May 2019, used a SIR-30 GPR towed by a 4-wheel autonomous vehicle, "Frostyboy", developed by the Polar Research Equipment group (Fig. 48). It was not able to detect the buried test fan hub, but this may have been the result of a number of compounding factors when attempting the test (such as radiofrequency interference from FrostyBoy's communication system). The SIR-30 GPR had no false positives (ice lenses with a signal similar to the buried test hub). Any of a number of factors could have contributed to this difference, such as the difference in measurement frequency, radar systems, tow vehicles, tow speed, or post-processing.

The SIR-30 400 MHz antenna was used to sound the ice sheet to depths of 40 m and identify snow-covered crevasses. During the survey of the most promising ONERA target during the field campaign, it detected a highly reflective surface at a rough depth of 3.4 m. The signal was seen again at the same location in two more surveys. Given that the SIR-30 had not seen any false positives outside the crevasse field, and the strong signal was the only one of its kind seen during the different crevasse assessment surveys, this signal was deemed promising. However, based on the GPR experience from the first field campaign, it was not certain that the signal came from a metallic object until a similar signal was observed with the SnowTEM detector.

Source: Austin P. Lines – PRE

Fig. 48: Frostyboy autonomous vehicle

The 400 MHz antenna was repeatedly hand towed nearby to further assess crevasses around the planned excavation site. It was determined that the fan hub could be seen when the GPR passed within 1.5 m of the part. Given the post-excavation measured burial depth of 3.3 to 4 m, this was consistent with the GPR beam pattern. In addition, the strong signal return on one side relative to the other was consistent in all GPR records that showed the anomalous diffraction. From knowledge gained during the excavation about the fan hub fragment's orientation in the snow, this stronger reflection was due to the different surfaces and orientation of the part. The reason for the GPR detection of the real fan hub but not the test fan hub may be due to their different sizes, given that their burial depths were similar.

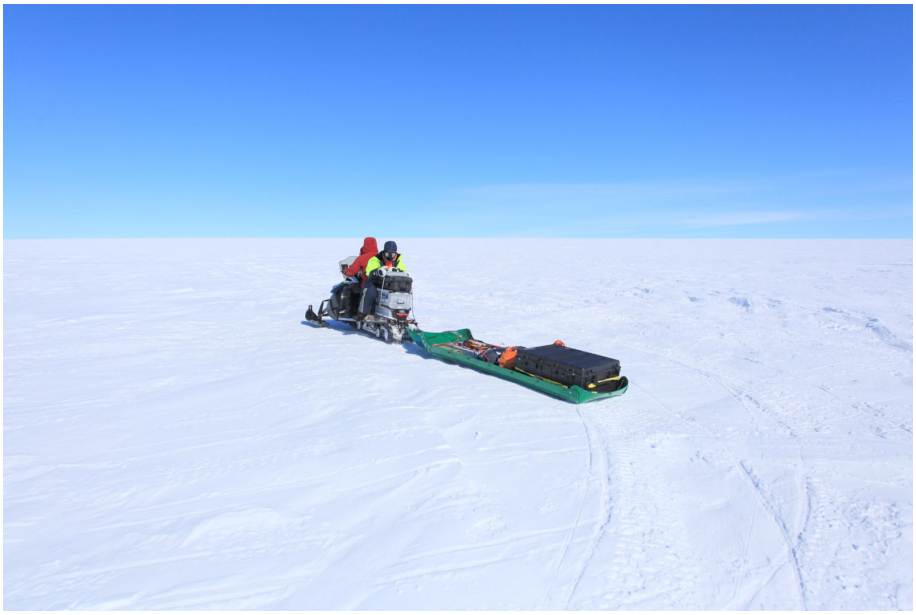

Source: GEUS

Fig. 49: Towing MALÅ GPR with snowmobile during first field campaign

Due to technical issues during the test in Zermatt, the functionality of the electromagnetic sensor SnowTEM was first empirically verified in the field. The flags marking the test hub buried at the end of CR1 were finally buried as well so detecting and locating the buried test hub at the beginning of CR2 was a good test to evaluate SnowTEM capabilities. It appeared that the test piece was not detected while moving over it, but when stationary, SnowTEM found it buried at a depth of 4.2 m. While moving, noise levels increased by 50 to 100 %, due to motion induced current.

The survey of targets 2a and 2b was then performed by driving 1 to 2 m spaced tracks and stopping for a few seconds every meter.

Because it was deemed unreasonable to safely move the SnowTEM sensor and all other necessary equipment to target 1 by snowmobile over the eleven crevasses separating the camp and the target, a SnowTEM setup was created which could be transported by helicopter and pulled manually. The modified SnowTEM worked identically to the original, albeit with some difficulty in maintaining the constant geometry between transmitter and receiver coils. Near where the SIR-30 GPR detected an anomalous feature, a signal about two orders of magnitude higher than from the buried test piece was detected, indicative of buried metal. The SnowTEM localized the fan hub fragment ~1 m north of a crevasse ~4 m wide with a ~6 m thick bridge. The signal was much stronger than from the test fan hub fragment due to a combination of it being a larger part, at a shallower depth, and with additional non-titanium parts attached to the fan hub fragment: carbon fiber composite, aluminum, Teflon, and stainless steel.

The signal was strong enough for this fan hub fragment to have been detectable with the SnowTEM in motion even with the increased motion-induced noise. The fan hub fragment was clearly detectable over an area greater than 32 m^2 – when it was within the 16 m2 transmitter coil, in a similar area between the transmitter and receiver coils, and still detectable outside this area.

In conclusion, the use of redundant, independent, and autonomous sensors is recommended. Redundancy is a common field technique to manage failures in hostile and remote locations. In this project, two identical SnowTEM systems were built to avoid impacting the project's success should there be a breakdown. Each GPR was also brought to the site with a complete redundant set of equipment.

The two different GPRs behaved similarly for 'traditional' GPR observations of deep ice layers, but differently with respect to the ice lenses in the firn.

Independent sensors are useful to cover a wide range of sensing capabilities for new target types outside the range of most glaciologists' experience, or for common target types that are buried in a material and environment outside the range of most airplane accident investigators' experience.

Independent sensors can also cover limitations of individual sensors. For example, GPRs are a common tool operated by diverse personnel with significant polar field experience, sniffer dogs (not used here) are commonly trained to detect human remains, RECCO detectors (not used here) are lightweight and hand-held, and the SnowTEM has a large ground footprint and can be used to distinguish conductive from non-conductive material.

Autonomous sensors should be used to reduce exposure to possibly high-risk work environments, increase the searchable area, or decrease the search time. In the near future, it is likely that heavy-lift-capable drones will be a useful new sensor platform for this type of field campaign.

5.4 Extraction

It was initially planned to extract the part at the end of CR2 if the part was located. Weather delays, specific hardware needs and staff member involvement in other projects prohibited the excavation of the part just after its detection. This allowed time to carefully organise the extraction campaign with the appropriate means and staff.

Out of the many concerns with regard to the excavation expedition, two concerns were deemed “major”:

- the safety of people working on the ice sheet: the part was 1 m from a crevasse lip, snow was starting to melt (it was end of June 2019), weakening the snow bridges over the crevasses,
- the preservation of the part, to enable a proper failure analysis once recovered. This required avoiding any metal-to-metal contact with the part.

To address the first issue, a team of mountain rescuers was gathered by Greenland Guidance. They were used to working in a glacier environment in the presence of crevasses, with ropes and associated safety gear.

For the second issue, a 120 kW Herman Nelson heater was rented to melt the snow surrounding the part. As eleven crevasses separated the detection location and the camp, the necessary equipment had to be moved to the excavation site by helicopter. An estimated 20 to 40 hours of digging to excavate the fragment was estimated.

The first layers of snow were removed with shovels and sleds towed by an electric winch. Ice layers formed by melted and refrozen snow during the past seasons had to be cut with chainsaws. The part was expected to be laying 4 m deep, but a metal-to-metal contact with a shovel occurred at a depth of 3.30 m. After that, only the heater was used to free the part. Surgical gloves were used while handling the fan hub to protect it from contamination from hands that had recently been in contact with a generator, winch, stove, or other engines that might complicate the investigation.

When the part was slung to Narsarsuaq Airport, an additional contact with a fan blade occurred after the part was on the ground when the helicopter, still hovering directly over it, released the net hooks. The metal net hook fell straight down and dented a fan blade. These impacts had finally no consequence for the failure analysis.

Despite all the precautions which were taken with the information available at that time, a nonzero level of risk of damaging the part still existed and had to be accepted.

The methodology chosen for the extraction allowed the part to be extracted in safe conditions in approximatively 30 hours with five people. The winch and the heater turned out to be essential.

5.5 Weather conditions

Both ground field campaigns were planned taking into account weather delays as their total length included a 20 % buffer day margin.

For CR1 in April-May 2018, 23 camping nights on the ice-sheet were planned, and 23 nights were effectively spent on-ice. Harsh weather was however encountered during the mission. During some storms, tents became buried by snow drift, and needed to be moved. At the end of the campaign, severe weather was encountered which resulted in some tents sustaining damage (bent or broken poles, zippers opening and snow drift inside), some being abandoned in the morning. White-out conditions occurred. Visibility was up to 2 to 3 m only (zero to one flag). Ropes were used to guide people from the sleeping tents to the kitchen tent. The toilet tent flipped and collapsed.

Despite these episodes, the team arrived at the site and left it as scheduled, which was rare enough to be noted. Temperatures ranged from -35 °C to 0 °C. Windy days could result in a wind chill of -50 °C.

For CR2 in May-June 2019, 24 camping nights were planned. Only 10 were spent on-ice. Helicopter flights were planned for certain days in advance. Due to high winds or clouds or both at Narsarsuaq, on the search site, or in-between, lots of flights had to be cancelled or rescheduled when possible, depending on helicopter availability. The initial planning envisaged the complete team being on site on 28 April 2019. In reality, because of weather hold-ups, almost nothing happened before 11 May when the last slings of hardware and five people were finally flown to the search site. Once on site, 20 to 30 % of the remaining days were still unworkable due to storms, and each storm required several hours of work to deal with snow drifts and buried equipment (Fig. 50). Temperatures ranged from -15 °C to +5 °C.

The extraction phase was initially planned as follows: two days to sling gear in and transport people to the extraction site, four days of digging, and two days to sling out and leave the camp, with four buffer days. No camping on-ice was planned, the campaign was based on flights in and out to transport the workers based at the hotel in Narsarsuaq. Helicopters were booked for almost every day from 24 June to 8 July. Due to weather hold-ups, the first flight in occurred on 28 June, meaning that the 4-day margin was already consumed. Once on ice, the decision was made not to fly out in the evening as weather was getting worse but to use the remaining gear from CR2 to camp on the ice. The crew remained on ice for 3 nights and flew out without any other weather delay.

In conclusion, even if margins were taken, the weather is not very predictable nor manageable in this area of the planet and can lead to weather hold ups. While the helicopter is the most convenient way to get to the search zone, it is particularly affected by weather conditions, whether in Narsarsuaq, in the search zone or between the two.

Weather hold ups at the beginning of CR2 led to a degraded campaign compared to what was initially planned. Constant adaptation was essential in these situations.

Fig. 50: Blowing snow burying equipment during a strong wind episode

6 - CONCLUSION

After 21 months of extensive searches, using advanced technologies such as synthetic aperture radars, satellite imagery, ground penetrating radars, electro-magnetic sensors, an autonomous vehicle and, above all, with the commitment, knowledge and experience of all the people involved, a fan hub fragment from engine No. 4 of the A380-861 registered F-HPJE was finally found and recovered.

Dedicated developments were made during this period. The SAR operated by ONERA from an AVDEF airplane had never been used in an arctic environment before. Because of unexpected backscatter noise on the radar images, and because of the presence of crevasses and ice lenses in the search region, dedicated image-analysis algorithms had to be developed after the aerial radar campaign. This post-processing made it possible to locate a fan hub fragment under the snow in one of the priority search areas defined by ballistic computations. This achievement required a tremendous amount of persistence on the part of ONERA staff given the initial results.

In addition, an existing transient electro-magnetic system used to map water networks under the soil surface was improved to detect a piece of titanium under snow and ice. Associated with GPR and a 4-wheel autonomous vehicle, the sensors confirmed the location of the part determined by ONERA. The field work team members led by GEUS showed an incredible adaptability to overcome the complications encountered over the course of the successive campaigns and to deal with weather delays.

The extraction phase used mountain rescuers to safely dig out the part which was found 3.30 m below the surface, at one meter from a crevasse.

The fan hub fragment was transported to Narsarsuaq by helicopter, then to Pratt & Whitney's facilities in East Hartford, CT, USA, for a detailed examination supervised by the BEA.

Finding this fragment was key for determining the root cause of the engine failure. An Annex 13 safety investigation report will be made available to the public on the BEA website in mid-2020.

The success of these operations has to be attributed to the exemplary cooperation between stakeholders, ranging from small contractors and PhD students to some of the world's largest aerospace and defense companies. Relying on the best specialists in the fields of glaciology, arctic expeditions, radar imagery and electro-magnetism was also key to the success, as much for their ability to operate the dedicated technologies as for their ability to deploy and carry out their mission in such a harsh environment. The skills and resourcefulness of the various team members most certainly contributed to the success of this multi-phase operation.

Grateful thanks are due to all those who financially contributed to this project and to all who participated in one way or the other.
Special thanks are addressed to the AIB DK for their continuous help, in particular for their involvement with the Greenland authorities which significantly facilitated the BEA's work.

REFERENCES

BEA. (2019). *TECHNICAL REPORT - Accident to the Airbus A380 registered F-HPJE and operated by Air France on 30/09/2017 en route over Greenland - October 2017 - June 2018 - Searches Phase I & II.*

Benson, C. S. (1962). Stratigraphic studies in the snow and firn of the Greenland.

Crider, D. (2015). Trajectory Analysis for Accident Investigation. *AIAA Modeling and Simulation Technologies Conference, AIAA SciTech Forum*.

DiMarzio, J. P. (2007). *GLAS/ICESat 1 km Laser Altimetry Digital Elevation Model of Greenland, Version 1.* . Boulder, Colorado USA - NSIDC (National Snow and Ice Data Center).

Edward Josberger, W. B. (n.d.). *Fifty-Year Record of Glacier Change Reveals Shifting Climate in the Pacific Northwest and Alaska, USA.* Retrieved from USGS: http://ak.water.usgs.gov/glaciology

Joughin, I. B. (2010). Greenland Flow Variability from Ice-Sheet-Wide Velocity Mapping. *Journal of Glaciology 56*, 415-430.

Joughin, I. B. (2015, updated 2018). *MEaSUREs Greenland Ice Sheet Velocity Map from InSAR Data, Version 2.*

Karlsson NB, C. W. (2019). Ice-penetrating radar survey of the subsurface debris field at Camp Century, Greenland. *Cold Regions Science and Technology*.

Mankoff, K., Van As, D., Lines, A., Bording, T., Elliott, J., Kraghede, R., . . . Karlsson, N. (2020). Search and recovery of aircraft parts in ice-sheet crevasse fields using airborne and in situ geophysical sensors. Journal of Glaciology, 66(257), 496-508. doi:10.1017/jog.2020.26

Paterson, W. (1994). *The Physics of Glaciers (3rd ed.).*

BEA

Bureau d'Enquêtes et d'Analyses
pour la sécurité de l'aviation civile

10 rue de Paris
Zone Sud - Bâtiment 153
Aéroport du Bourget
93352 Le Bourget Cedex - France
T : +33 1 49 92 72 00 - F : +33 1 49 92 72 03
www.bea.aero

RÉPUBLIQUE
FRANÇAISE
Liberté
Égalité
Fraternité